Minerals Engineering 206 (2024) 108539

Contents lists available at ScienceDirect

Minerals Engineering

journal homepage: www.elsevier.com/locate/mineng

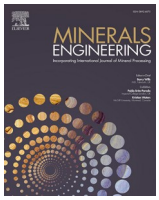

Detailed characterisation of precious metals and critical elements in anode slimes from the Olympic Dam copper refinery, South Australia

Nigel J. Cook [a,*], Kathy Ehrig [a,b], Cristiana L. Ciobanu [a], Samuel A. King [a], Vanessa Liebezeit [b], Ashley D. Slattery [c]

[a] School of Chemical Engineering, The University of Adelaide, Adelaide S.A. 5005, Australia
[b] BHP Olympic Dam, 10 Franklin Street, Adelaide S.A. 5000, Australia
[c] Adelaide Microscopy, The University of Adelaide, Adelaide S.A. 5005, Australia

ARTICLE INFO

Keywords:
Minor metals
Copper anodes
Electrorefining
Anode slimes
Characterisation
Olympic Dam

ABSTRACT

Together with silver (Ag) and gold (Au), which are almost always recovered, the impurity elements, arsenic (As), antimony (Sb), bismuth (Bi), tin (Sn), lead (Pb), selenium (Se) and tellurium (Te) are major components of anode slimes, a by-product of the electrorefining of impure copper. The Olympic Dam electrorefinery, South Australia, generates raw slimes (~30 % Cu, 5–10 % Ag, 0.5–1 % Au, 3–4 % Bi, ~2–3 % Sb, and 5–6 % As), which subsequently undergo decopperisation and then pH-neutralisation. Decopperisation involves treatment with steam and acid at 90 °C, giving a slime that contains ~ 1 % Cu, 8–17 % Ag, ~2% Au, ~7% Bi, ~4–5 % Sb, and ~ 3 % As. pH-neutralisation is achieved by addition of NaOH and is the final step prior to cyanidation and precious metal recovery.

Bulk chemical compositions, gross morphology and particle size distributions are complemented by high-magnification backscatter imaging and energy-dispersive X-ray analysis of individual particles in raw, decopperised, and pH-neutralised anode slimes. In a first micron-to-nanoscale approach, we use electron backscatter diffraction mapping to assess the crystallinity of individual component phases and a scanning transmission electron microscopy study on micron-sized slices extracted *in-situ* to confirm the crystal structure of a conspicuous $BiAsO_4$ phase as rooseveltite. The results establish an in-depth understanding of element deportments in slimes and their evolution during sequential stages of treatment. Characterisation studies for Te, Se, Sb, Bi, and As are essential prerequisites for any design of metallurgical circuits for by-product recovery from anode slimes and/or electrolyte. This study aims to demonstrate that complementary cutting-edge microanalytical techniques widely used in mineralogy provide a level of detail essential when considering refinery slimes as a new source of critical commodities.

1. Introduction

Expectations for high-quality metal products containing minimal impurities and the accelerating demand for many minor metals are the twin drivers of current research addressing the distribution of minor metals in ores, concentrates and mine tailings, and their behaviour through smelter and refinery circuits. Several elements that commonly occur in minor amounts within copper sulphide ores, including silver (Ag), gold (Au), arsenic (As), antimony (Sb), bismuth (Bi), tin (Sn), lead (Pb), selenium (Se) and tellurium (Te), report to concentrate after froth flotation, and will accumulate within anode slimes after smelting and subsequent electrorefining (Schlesinger et al., 2021). Silver, Au, platinum group metals (if present in the feed) and in many cases also Te, are routinely recovered from anode slimes (e.g., Hoffmann, 1989; Cooper, 1990; Chen and Dutrizac, 1996; Swinbourne et al., 1998; Hait et al., 2009). Although the traditional emphasis has been on ensuring the removal of all impurities, and thus guaranteeing high-purity cathode and optimal recovery of precious metals, there is a growing awareness of the potential economic opportunity offered by the recovery of Sb, Bi, and even As from refinery slimes and electrolyte, as well as Te in operations where it is not already recovered (Moats et al., 2021; McNulty et al., 2022; Nassar et al., 2022). These Group 5A elements have been traditionally regarded as unwanted, deleterious components of copper ores (e.g., Lane et al., 2016), they are now internationally viewed as

* Corresponding author.
E-mail address: nigel.cook@adelaide.edu.au (N.J. Cook).

https://doi.org/10.1016/j.mineng.2023.108539
Received 11 September 2023; Received in revised form 28 November 2023; Accepted 11 December 2023

"critical minerals" (IEA, 2023). Critical minerals are important for many advanced, low-emission technologies such as electric vehicles, wind turbines and solar panels, yet are subject to supply chain risks and geopolitical concerns.

The composition and phase chemistry ('mineralogy') of anode slimes from different refineries around the world have been dealt with extensively, notably in the landmark series of papers by Chen and Dutrizac (1987, 1988a, 1988b, 1989a, 1989b, 1989c, 1990, 1991, 1993, 1996), Scott (1990), and later works by the same authors and/or their Canadian colleagues (Scott, 1990; Chen and Dutrizac, 2003, 2004, 2005, 2008; Beauchemin et al., 2008). Additional data from refineries worldwide, coupled with experimental approaches, has advanced understanding of slime precipitation, slime compositions, and the methodologies and parameters required for optimised recovery of residual copper, precious metals and other contained elements from slimes and electrolyte (Hoffmann, 2004; Wang et al., 2006; Moats et al., 2012, 2019; Mastyugin and Naboichenko, 2012; Aguilera et al., 2015; Steinlechner, 2018; Xing et al., 2019; González de las Torres et al., 2021).

More recent studies have recognised the unrecovered value in anode slimes and identified potential routes for their recovery (Zeng et al., 2022, 2023). Some of these studies have emphasised the importance of slimes characterisation for development of recovery methodologies (Kanari et al., 2019, 2020; Khakmardan et al., 2023). Techniques used in these studies have ranged from traditional methods like backscattered scanning electron microscopy, energy-dispersive X-ray spectroscopy (EDS), and X-ray diffraction (XRD). Relatively few of the modern studies have sought to obtain quantitative compositional data on individual component phases, or have taken a mineralogical approach that also addresses the textures and relationships between precipitate phases at the micron-scale.

A study of refinery slimes from one of the world's largest copper mining-processing-smelting-refining operations is thus opportune. The Olympic Dam mine in outback South Australia exploits a breccia-hosted sulphide ore deposit for Cu, U, Au and Ag (Ehrig et al., 2012, 2017). The on-site metallurgical plant (BHP Billiton, 2009) produces 99.9999 % pure copper cathodes, U_3O_8 concentrate, and gold and silver bullion. Despite interest in the diverse range of other elements in refinery slimes from Olympic Dam, no characterisation work has been published in the public domain prior to the present work.

The present contribution reports the results of a systematic study of raw, decopperised, and pH-neutralised anode slimes from the Olympic Dam electrorefinery. Our examination of anode slimes is able to take advantage of the advances in analytical sensitivity and spatial resolution unavailable at the time of seminal research in the field thirty years ago (*op. cit.*). Instead of relying on bulk characterisation methods such as XRD ill-suited to the identification of amorphous phases, we employ contemporary microanalytical methods that focus on the morphology, composition and association of individual particles. We also introduce two cutting-edge methods widely used in mineralogy and materials science to enhance understanding of slimes phases at the requisite scales: electron backscatter diffraction (EBSD, e.g., Schwartz et al., 2000; Humphreys, 2001) to enable rapid assessment of phase crystallinity in individual particles; and scanning transmission electron microscopy (S/TEM; Pennycook and Nellist, 2011) in high-angle annular dark field (HAADF) mode to visualise the structures of crystalline phases.

The objectives are firstly to describe refinery operations at Olympic Dam, document bulk compositions in recent and past slimes, and evaluate the physical form and chemical speciation of Ag, Au, As, Sb, Bi, Sn, Pb, Se, and Te. We document how their distributions evolves through sequential slime treatment processes. Secondly, we show how state-of-the-art methodologies from mineralogy can be applied to challenging materials like anode slimes, where an adequate understanding of phase chemistry is an essential precursor for the successful development of any new processing methodology.

2. Olympic Dam operations

Olympic Dam is a giant iron-oxide copper gold (IOCG)-type ore deposit. Alongside the revenue commodities copper, uranium, gold and silver, the breccia-hosted sulphide deposit is also enriched in a broad range of other elements, including As, Ba, Bi, Cd, Co, Cr, Nb, Ni, Sb, Se, Sn, Sr, Te, V, W, Y, and rare earth elements (REE) (Ehrig et al., 2012, 2017). Ore minerals are characteristically fine-grained and intergrown with one another, forcing optimisation of metallurgical performance at Olympic Dam through a comprehensive knowledge of mineralogy. Physical relationships between minerals down to the sub-micron-scale and in-depth deportment balances for trace elements are shown to assist with recovery and ensure consistent concentrate quality.

Geochemical and mineralogical characterisation of the deposit over the past 30 years has allowed an appreciation of mineralogical variation at the deposit-scale and has resulted in an extensive inventory of more than 120 minerals (Ehrig et al., 2012). This cumulative work has also addressed the mineralogical deportment and petrography of Se, Te, Bi, Sb, As, Co, Ni, etc. in the orebody. For example, a dozen or more independent selenide and telluride mineral phases are reported (including Ag-, Ag-Au-, Bi, and Ag-Bi-selenide/telluride species), with Se and Te also observed to occur in solid solution within the common Cu-(Fe)-sulphide minerals (authors unpublished data).

Silver, Au, As, Sb, Bi, Sn, Pb, Se, Te, and most other minor metals report to copper concentrates during conventional froth flotation. After concentrate leaching to recover uranium and remove fluorite, the concentrate is smelted in a two-stage operation (flash furnace followed by electric slag reduction furnace). Blister copper is delivered to an anode furnace where sulphur and residual oxygen are removed. Molten copper is cast into moulds. The above minor elements typically report to anode copper. Insights into the distribution of minor elements in copper anode, both dissolved in copper metal and as micron-scale inclusions, will be published elsewhere (Cook et al., in review). Those contributions show that the above elements occur in solid solution within copper metal as well as inclusions, albeit in significantly different proportions from element to element, and that anode impurity inclusions are dominated by cuprite, Cu-selenides (containing subordinate Te), and various Cu-Bi-As-(Pb)- and Cu-Bi-Sb-oxides.

The Olympic Dam refinery consists of the electrorefining (ER) and electrowinning (EW) tank houses and a slimes treatment plant. Copper anodes from the smelter containing ~ 99.7 % copper are prepared to ensure verticality, sorted to ensure measurement tolerances are met, milled, and transferred to the on-site refinery for conversion to high-grade (>99.99 %) copper cathodes (BHP Billiton, 2009). Anodes are loaded into ER cells. The electrorefining process operates on a ten-day cathode, twenty-day anode cycle and involves dissolution of impure copper anodes (each 365 kg in weight, in batches of 56 anodes) into an electrolyte ($CuSO_4$-H_2SO_4-H_2O; ~45 gpl Cu, 170 gpl H_2SO_4, 63 °C) by applying an electrical current (28,000 A; 0.3 V) between the anode and a stainless steel permanent cathode. Pure copper is plated onto the mother stainless-steel cathode and soluble impurities dissolve in the electrolyte. Impurity elements (Au, Ag, Bi, As, Sb, Sn, Pb, Te, Se, etc.) precipitate and accumulate in so-called anode slimes at the bottom of the electrolytic refining cells. Some elements (notably As, Sb, and Bi) are generally soluble and may only precipitate once saturation levels are reached. Reagents are continually added to ensure electrolyte quality control and to maintain copper concentration. Filters are used to maintain electrolyte clarity and reduce cathode impurity contamination from fine slimes. At the end of each cycle, the anodes are washed of slimes and returned to the smelter as scrap anodes. Scrap represents around 15 % of the original anode weight. Cathode copper, now without impurities except for 7–8 ppm silver, is stripped from the mother plates, bundled into 3 tonne-bundles and sold on to customers.

Anode slimes are emptied from the cells every 20 days. Each batch of slimes (750–800 kg) is washed and fed to a slurry storage facility prior to pressure filtration. The resultant solids are then sent to a

decopperisation tank where they are treated with steam and H_2SO_4 at 90 °C under atmospheric pressure to remove Cu. The decopperised slimes are filtered, washed, and sent for neutralisation with caustic soda. The Cu-bearing electrolyte is returned to the hydrometallurgy circuit, ultimately being recovered by electrowinning. The refinery process is illustrated schematically in Fig. 1. Neutralised slimes are sent for cyanidation in roughly 1000 kg batches yielding a liquor containing gold and silver and rejecting any Pb and radiogenic $^{210}Pb/^{210}Po$. Process design in the precious metals refinery is focussed on the removal of radionuclides to produce high quality gold and silver bullion.

The slurry is subjected to a modified Merrill-Crowe process, followed by roasting to doré as a first step to recovery of precious metals (gold and silver). Further details are given by Hall (1993).

3. Samples and methodology

Representative samples of raw tank-bottom anode slimes, decopperised slimes, and pH-neutralised slimes were collected from the Olympic Dam refinery in September 2022. All samples were assayed for a suite of 67 elements at Genalysis-Intertek (Adelaide), involving six different analytical methods (see footnote to Table 1). Note that materials from some individual batches were combined to be more representative.

Selected samples were mounted in epoxy, polished with diamond paste, and finished using colloidal silica. Although most of the imaging reported here was made on unsized material, selected raw and decopperised slime samples were cyclosized to remove most of the < 5 μm-size material prior to mounting, in order to generate a sample better suited for imaging and subsequent microanalysis by electron microprobe, albeit less representative of bulk composition.

Each sample was imaged using a FEI Quanta 450 FEG Environmental Scanning Electron Microscope (Adelaide Microscopy, The University of Adelaide). The instrument was operated in backscatter electron (BSE) imaging mode to identify phases, document textural relationships, and obtain semi-quantitative compositional data using the in-built X-ray dispersive spectrometer.

Assessment of phase crystallinity in individual particles with known composition was made by electron backscatter diffraction (EBSD) on a FEI-Helios nanoLab dual focused ion beam and scanning electron microscope (FIB-SEM) platform in the same laboratory. Samples were polished in a colloidal silica suspension and a thin (2.5 nm) carbon coat was applied prior to analysis. EBSD data was collected using an Oxford Symmetry S3 detector which operated at 20 kV and 2.7nA. Initially, spot analyses were applied on all phases to acquire Kikuchi diffractions indicative of phase crystallinity. Maps were then taken from representative areas in selected crystalline phases to produce Band Contrast (BC), Inverse Pole Figure (IPF) and phase maps of indexed minerals. Post-processing was performed using AZtecCrystal software to reduce data noise. Given that a large part of the slimes was found to be amorphous, no bulk XRD determinations were made.

Thinned foils containing a crystalline Bi-As-oxide were prepared for nanoscale study on a FEI-Helios nanoLab Dual Focused Ion Beam and Scanning Electron Microscope (FIB-SEM) platform in the same laboratory. The nanoscale study was carried out using an ultra-high resolution, probe-corrected, FEI Titan Themis S/TEM, in high-angle annular dark field (HAADF) mode equipped with an energy-dispersive spectroscope (EDS) detector. Image acquisition was undertaken using FEI software, TIA (v4.15) and complementary imaging by drift-corrected frame integration package (DCFI) included in Velox (v. 2.13.0.1138) software. Radial Wiener, High-pass, Average and Gaussian blur filters were used to eliminate noise and/or enhance the images. Diffraction pattern indexing was done with WinWulff© (v1.6) (JCrystalSoft) and publicly available data. CrystalMaker® (v10.5.7) was used to generate crystal structure models; image simulations were created using STEM for xHREMTM (v4.1) software. All EDS data acquisition and processing was carried out using Velox software.

4. Bulk compositions

Table 1 gives representative assays for a selection of the raw, decopperised, and pH-neutralised slimes samples studied here. Major components are Au, Ag, As, Bi, Cu, Pb, Sb, Se, Sn, Te, Al, Ba, Fe, and Si, with subordinate (ppm-level) Co, Ni, Cr, and Sr. The concentrations of individual components can vary significantly between individual batches and there are also marked differences between different size fractions. It should however be pointed out that the coarsest + 53 μm fraction is generally far smaller in volume than the fine fraction.

The coarsest fractions contain markedly more Al, Ba, Cr, Fe and Si (elements added during processing or from scrap or other artificial origin), and lesser Au, Ag, Pb, Se and Te, which are preferentially in the –C5 fraction. Bismuth, Sb and Sn are also higher in the coarse fractions due to their partial occurrence within coarser 'sediment-like' fragments (see description below).

Decopperisation of slimes results in the loss of about one-third of the material (~30 % Cu) to electrolyte, giving an apparent increase of most other elements. Arsenic concentrations also drop in absolute terms, by around half, during the process of copper removal.

5. Slime characterisation, textures and main components

The greater part of all slime samples is ultra-fine-grained (typically < 10 μm), often agglomerated in the mounted samples, and, in BSE images (Fig. 2A, B, C), dominated by small bright structures within a darker, albeit visibly heterogeneous 'matrix' (following terminology used by Chen and Dutrizac in early papers – the matrix is referred to as 'oxidate' in some later papers). Each sample also contains a small

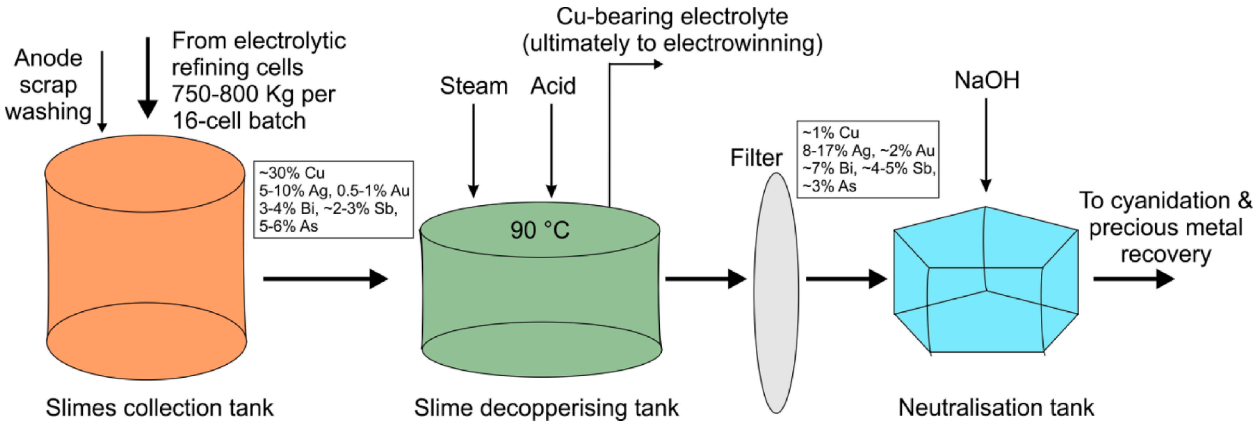

Fig. 1. Simplified schematic diagram of slimes circuit at Olympic Dam (sourced from unpublished BHP documents).

Table 1
Assay data for elements of interest in slimes samples (data in ppm unless otherwise stated).

	Au	Ag	As	Bi	Co	Cu	Ni	Pb	Sb	Se	Sn	Te	Al (%)	Ba	Cr	Fe (%)	Si (%)
Raw slimes (sample 6100)																	
+53 μm	6479	52,662	56,559	44,421	174	216,689	111	32,593	35,441	63,914	5920	18,124	3.73	49,678	818	0.51	5.51
+C5	9222	69,350	65,899	32,839	257	313,414	120	39,061	22,071	83,258	1871	24,411	2.66	26,468	93	0.19	0.18
-C5	10,396	94,112	64,023	37,822	128	331,028	35	52,046	23,257	106,153	2065	32,332	0.54	6367	41	0.07	0.11
Raw slimes (older sample)																	
+53 μm	7574	41,579	48,754	36,747	196	248,194	430	32,016	46,646	72,761	4123	17,301	7.13	57,576	326	0.15	1.03
+C5	8989	50,022	58,733	26,983	218	299,836	397	35,892	30,951	79,834	2308	19,122	6.25	45,931	92	0.16	0.17
-C5	11,055	70,486	60,158	28,116	67	376,278	90	39,603	26,623	127,939	2232	31,320	0.82	10,027	46	0.07	0.09
Raw slimes [6101 (tank 1) + 6102 (tank 2), 1–10 Sept. 2022, batch nos. 17370, 17372]																	
6101B, unsized	11,583	90,934	52,743	37,371	216	296,024	88	53,221	24,178	112,682	2438	34,106	1.90	18,622	131	0.11	0.38
6102B, unsized	10,138	83,888	63,763	38,666	204	310,101	71	47,708	25,460	98,042	2443	30,521	1.82	18,288	133	0.09	0.64
6101 + 6102, +C5	11,957	76,408	63,142	19,924	284	339,124	91	43,901	16,789	97,842	2015	29,699	2.19	23,033	61	0.13	0.10
6101 + 6102, -C5	11,931	95,887	59,427	29,063	126	331,123	31	65,482	20,928	125,759	2959	36,050	0.62	7437	42	0/08	0.11
Decopperised slimes [6161 (tank 1) + 6162 (tank 2), 1–10 Sept. 2022, batch nos. 17370, 17372], [6163 (tank 3)]																	
6161, unsized	22,657	176,571	26,648	72,397	387	5685	162	105,383	44,036	215,765	4309	36,831	3.30	33,715	131	0.18	0.36
6162, unsized	20,748	170,348	29,936	78,811	435	3313	157	96,820	49,966	150,185	4264	35,903	3.41	33,038	160	0.17	0.59
6163, unsized	21,007	173,405	27,187	71,978	408	3387	164	98,263	46,212	175,499	4399	35,196	3.58	33,226	130	0.18	0.57
6163B, unsized	21,927	171,861	28,068	71,253	427	13,846	193	100,795	44,426	174,817	4363	37,224	3.61	36,535	133	0.18	0.53
6161 + 6162, +C5	6353	80,265	19,864	38,080	799	9611	388	115,224	30,712	101,538	4311	19,966	11.78	113,812	316	0.44	0.34
6161 + 6162, -C5	30,530	209,733	26,089	54,327	281	12,713	56	116,574	41,015	266,940	5561	39,485	1.06	12,808	76	0.13	0.08
pH-neutralised slimes (6170 from 1 to 10 Sept. 2022, batch no. 17368)																	
6170B, unsized	23,729	188,017	30,095	72,441	389	12,276	115	111,532	43,038	207,458	4433	35,929	2.96	29,148	138	0.17	0.33
6170, +C5	11,267	93,147	20,773	49,023	844	5443	656	95,778	40,922	141,160	4302	25,936	10.03	95,283	237	0.40	0.45
6170, -C5	28,425	195,269	22,818	57,517	253	3928	86	122,057	42,462	246,940	4917	42,660	1.06	12,558	68	0.11	0.12

Minimum detection limits (in ppm unless otherwise stated): Au 0.005, Ag 5, As 5, Bi 1, Co 1, Cu 50, Ni 20, Pb 50, Sb 5, Se 50, Sn 2, Te 5, Al 0.01%, Ba 0.5, Cr 20, Fe 0.01%, Si 0.01%, Sr 0.2.

Concentrations of other minor elements in raw slimes (in ppm unless otherwise stated): Ca 0.03 %, Ce 4, CO_2 2–4 %, Cs 0.08, Dy < 0.5, Er < 0.3, Eu < 0.4, Ga < 5, Gd < 0.3, Ge < 1, Hg 500–1700 ppb, In 5–15, K 0.01–0.03 %, La ~ 3, Mg < 0.04 %, Mn < 0.007 %, Mo 3–13, Nb < 1.5, Nd < 1, Pd 2800–15200 ppb, Pr < 0.4, Pt 1600–10400 ppb, Rb < 1, Sc < 3, Sm < 0.2, Sr 130–1800, Th < 0.3, Ti < 0.02 %, Tl < 3, U_3O_8 < 0.8, Zn < 50 – 110, Zr < 4.

Concentrations of the following elements were consistently below their respective minimum limits of detection (in brackets, ppm unless otherwise stated): Be (0.5), Cd (0.2), Hf (0.1), Ho (0.02), Li (0.02), Lu (0.02), Na (0.01%), P (0.01%), Re (0.02), S (0.02%), Ta (0.1), Tb (0.02), Tm (0.05), V (5), W (1), Y (0.5), Yb (0.05), Zr (1).

Analytical methodologies: Fire-assay / optical emission spectroscopy (Au), Fire-assay / mass spectroscopy (Pd, Pt), Four-acid-HBr / mass spectroscopy (Ag, As, Bi, Cd, Co, Ge, In, Li, Ni, Pb, Re, Se, Te, Tl, Zn), four-acid-HBr optical emission spectroscopy (S), lithium borate fusion / optical emission spectroscopy (Al, Ca, Cr, Fe, K, Mg, Mn, Na, P, Sc, Si, Ti), lithium borate fusion / mass spectroscopy (Ba, Be, Ce, Cs, Dy, Er, Eu, Ga, Gd, Hf, Ho, La, Lu, Mo, Nb, Nd, Pr, Rb, Sb, Sm, Sn, Sr, Ta, Tb, Th, Tm, U_3O_8, V, W, Y, Yb, Zr), gravimetric analysis (CO_2).

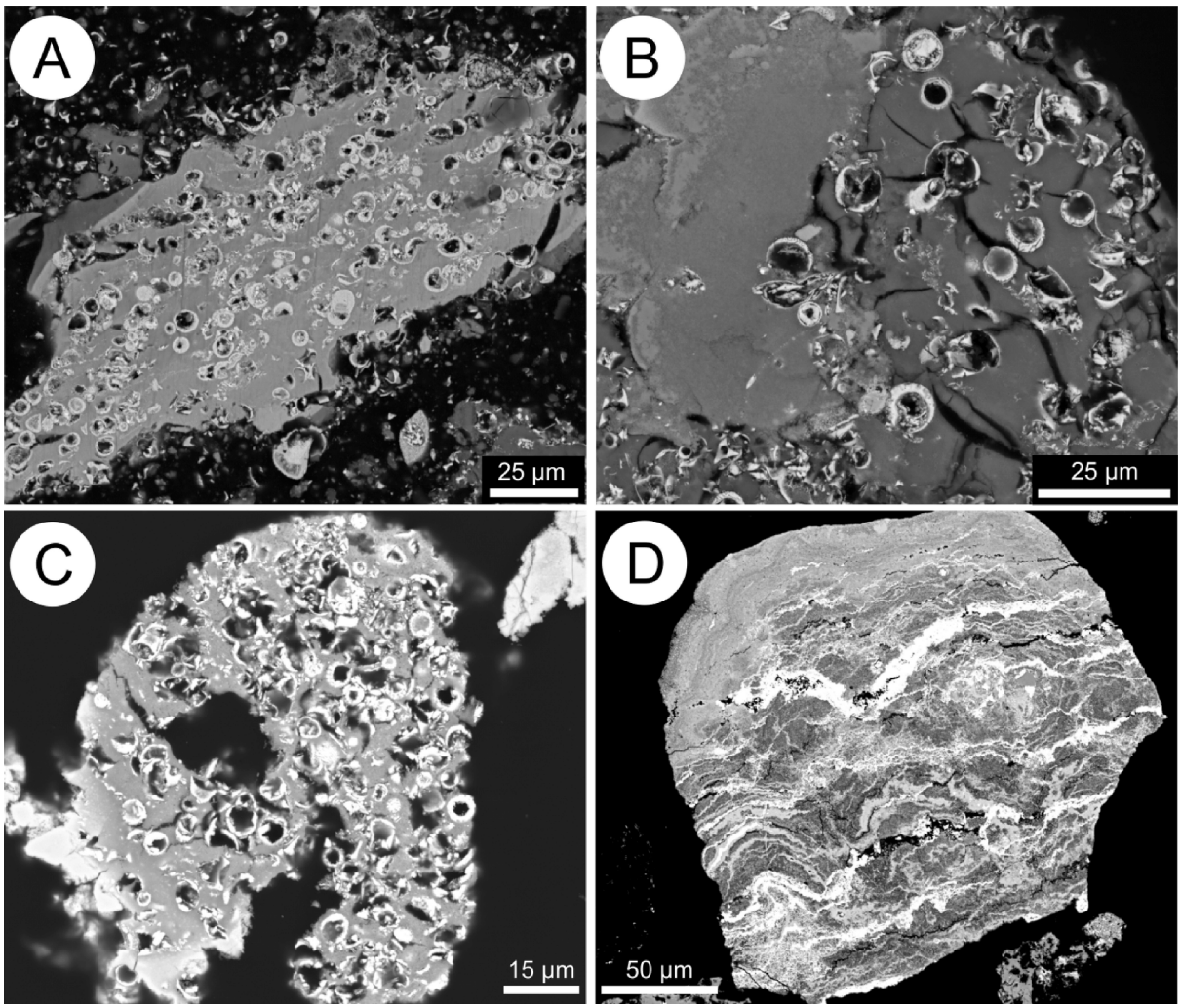

Fig. 2. Low-magnification BSE images of slimes. (A) Typical appearance of raw slimes: dense clusters of ~ 2–5 µm-sized spherical, ring- and atoll structures in colloidal matrix (35 % Cu, 8 % As, 8 % Se, 2–4 % S, minor Sb, Pb, Ag, and Te). Note that some ring structures are filled, while others are empty. (B) Raw slimes sample. Note heterogeneity in matrix domains with respect to composition (brighter domains contain greater Sb) and the variable density of the spherical, ring- and atoll structures. (C) Typical appearance of pH-neutralised slimes in which most spherical structures are empty. (D) Fragment from coarse size fraction of decopperised slimes featuring a conspicuous banded structure composed of a $BiAsO_4$ phase (bright), Bi-Sb-oxide (light grey) and a markedly darker grey Sn-bearing Bi-Sb-As-oxide phase.

proportion of larger composite particles that can be as large as 300–400 µm across (Fig. 2D).

The identified phases are grouped into four textural and compositional categories:

(i) Micron-sized ring- and atoll-like structures dominated by Cu-Ag- and Ag-selenides (in raw and decopperised samples, respectively), which are infilled, in part, by a $BiAsO_4$ phase and other Bi-As-(Sb)-oxides;
(ii) The amorphous, compositionally variable matrix hosting the ring- and atoll-like structures;
(iii) The $BiAsO_4$ phase, and other Bi-As-, Bi-Sb- and Bi-Sb-Sn-As-oxides, including free particles and species that comprise the conspicuous banded material in the coarser size fractions; and
(iv) An eclectic group of phases including Cl-bearing compounds, sulphates, alloys, silicates, and Al-bearing phases of techno- and anthropogenic origin that are concentrated in the coarsest size fractions.

This following description is intentionally brief and represents a simplified account of what are extraordinarily complex, polyphase and intimately intergrown materials. Detailed characterisation of each compositional-morphological group of phases, accompanied by high-magnification images, X-ray element maps, and quantitative electron probe analysis of selected phases, will be provided in a forthcoming sister paper.

5.1. *Atoll-like structures dominated by Cu-Ag- and Ag-selenides*

The most conspicuous feature in the raw slimes are the bright spheres, rings, and atoll-like structures composed of Cu-Ag-selenides (also containing Te and measurable Au) that sit within the amorphous Cu-As-dominant matrix that makes up the larger part of the slimes (section 5.2. below). These broadly circular features are typically 1–5 µm in diameter, exceptionally up to as large as 10 µm (Fig. 3A). In some cases, the selenides appear to have precipitated onto Bi-As-(Sb) oxide that fills the centre of the structure. In other cases, however, Bi-As-(Sb) oxides form an outer rim around the selenide (Fig. 3B). Many spherical structures are however empty, leaving a void surrounded by a ring- or atoll-like structure. Some of the spherical structures are not single grains but rather composed of aggregates of individual sub-µm-sized particles (Fig. 3C), apparently homogeneous in composition. Fine-grained $PbSO_4$

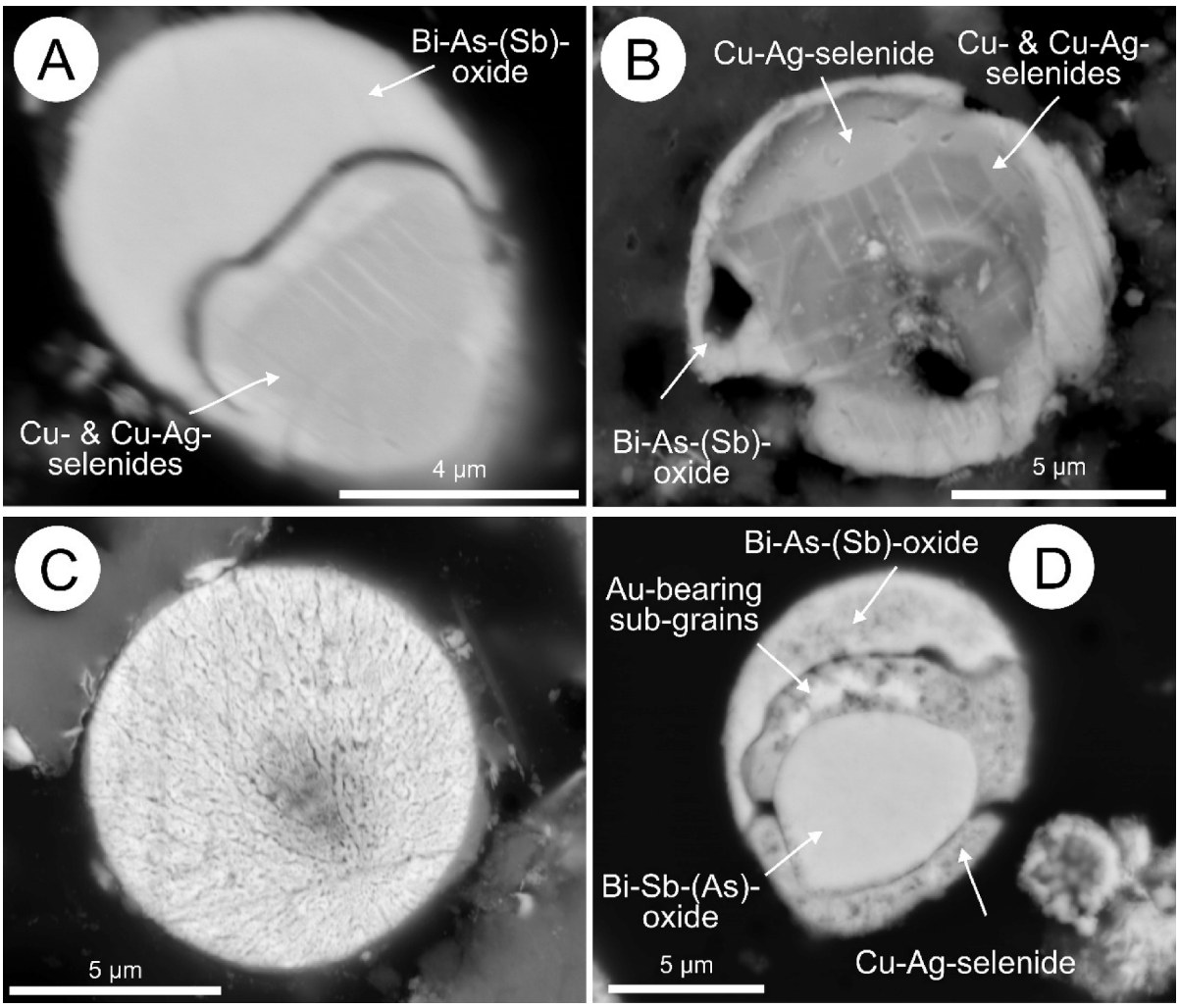

Fig. 3. BSE images showing detail of spherical and ring-like structures from raw (A-C) and decopperised slimes (D). (A) Composite structure in Cu-As-dominant matrix consisting of a hydrated (?) Bi-(Cu)-As-(Sb)-(Pb)-oxide (41 wt% Bi, 20 wt% O, 16 wt% As, 7 wt% Sb, 6 wt% Cu, 5 wt% Pb; normalised EDS data) and sub-micron-scale intergrowths of Cu- and Ag-Cu-selenides (dark and bright). (B) Sub-micron-scale intergrowths of Cu- and Ag-Cu-selenides, larger domains of Ag-Cu-selenide, and outer rim of Bi-As-(Sb)-oxide. (C) Spherical structure composed of an aggregate of fine sub-micron-sized Cu-Ag-selenide particles. (D) Example of complex spheroidal structure from decopperised slimes, in which both Bi-As-(Sb)- and Bi-Sb-(As)-oxides are recognised, and where Ag-selenides contain tiny Au-bearing sub-domains.

may, however, occur between the aggregated grains and readily accounts for the several wt.% Pb and S present in many EDS analyses.

In raw slimes, the atoll-like phases correspond to Cu-Ag- and Ag-(Cu)-selenides, always with subordinate Te. Ag:Cu ratios vary widely but Se/Te ratios are typically quite constant (around 3:1 to 4:1). The majority appear monophase but in some slightly larger particles, high-magnification images allows identification of coexisting Cu-Au and Ag-Cu-selenides, rarely extending to intricate graphic exsolution intergrowths of compositionally distinct selenide species (Fig. 3A, B).

EDS mapping indicates that gold occurs in solid solution within Cu-Ag- and Ag-selenides at concentrations of up to a couple of wt.%, and after decopperisation, as discrete microgranular inclusions of $Ag_3Au(Se,Te)_2$ (fischesserite or a closely related phase), seldom more 1 μm across contained within the selenides (Figs. 3D, 4).

Partial or total dissolution of infill is more pronounced in the decopperised slimes, leaving fewer well-preserved spherical structures. Only a minority of the atoll-like structures remain infilled. Cu-Ag-selenides are largely dissolved and replaced by Ag-selenides during decopperisation. The proportions of Se to Te are, however, broadly the same. Many of the larger Ag-selenides retain a few wt.% Cu, and a restricted number of Cu-Ag-selenides are observed to survive decopperisation. The Ag-selenides in decopperised slimes often appear more heterogeneous than in the raw slimes, are often decomposed or intimately intergrown with $PbSO_4$.

Small, brighter sub-grains, seldom more than fractions of a micron in size, within some spheroidal or atoll-like structures in both raw and decopperised slimes contain measurable concentrations of Au up to more than 10 wt% (Fig. 3D). These are tentatively assigned to a phase with a fischesserite-like composition (Ag_3AuTe_2).

Accompanying phases in the spherical structures are various Bi-As- and Bi-Sb-(As)-oxides, including $BiAsO_4$, although a few Cu-Bi-arsenates were also observed in raw slimes. These phases are typically homogeneous at the scale of the electron beam but may show evidence of decomposition. Small inclusions of a $BiSbO_4$ phase within $BiAsO_4$ are common. In decopperised slimes, Bi-As-oxides still predominate but the abundance of Bi-Sb(As)-oxides increases relative to in raw slimes.

Further degradation of the spherical structures is seen in pH-neutralised slimes. Most are fragmented or partially leached, lending the samples an almost breccia-like appearance.

5.2. *Colloidal matrix*

Although the spherical structures are the most conspicuous, the colloidal matrix hosting the spherical structures is arguably the largest

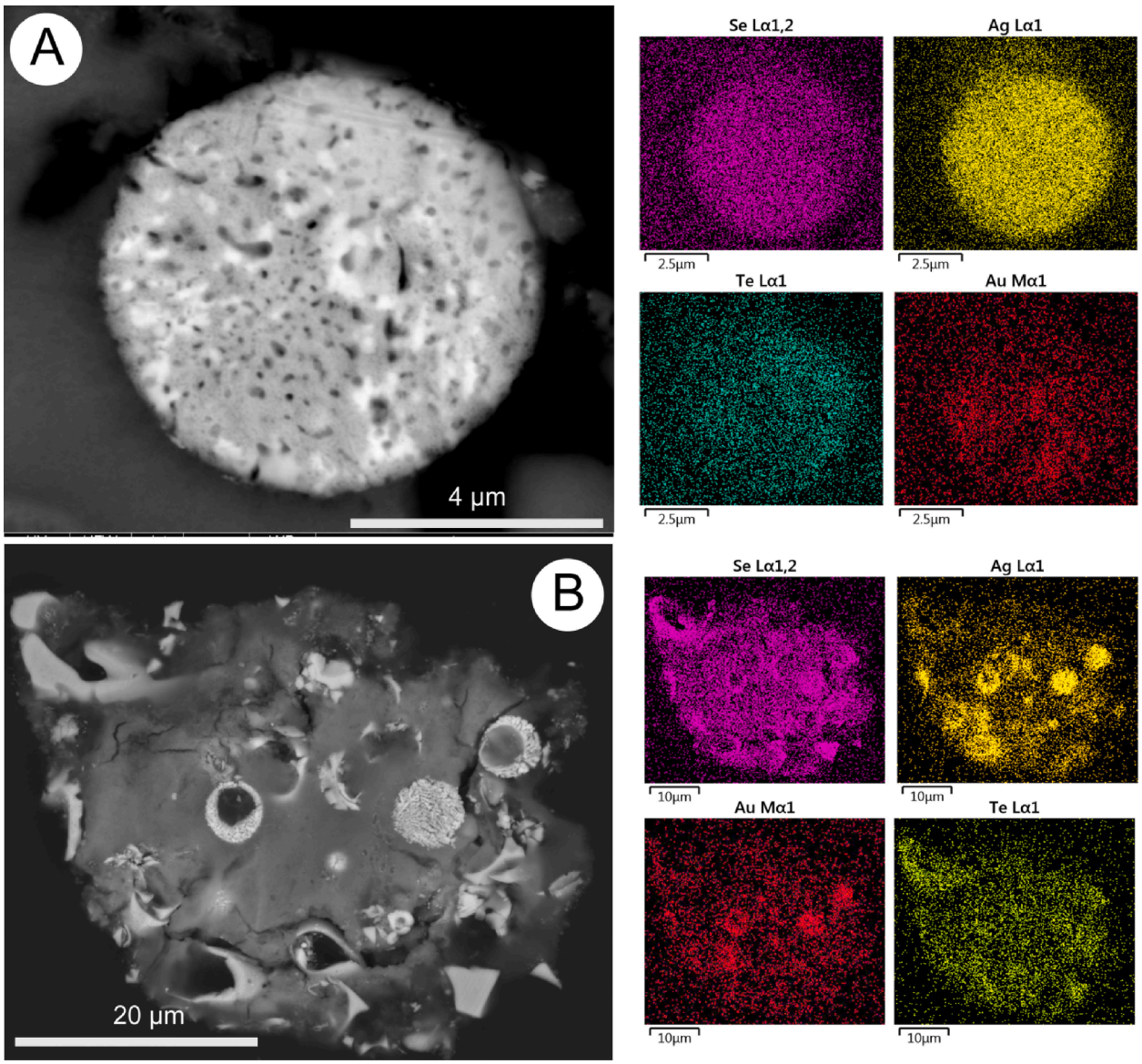

Fig. 4. (A) BSE image and EDS element maps showing distributions of Au, Ag, Se, and Te within spherical structures and host Cu-As-dominant matrix. Note Au enrichment in spherical structures but lower Au concentrations also in matrix (raw slime sample 2, +C5 fraction). (B) BSE image and EDS element maps showing distributions of Au, Ag, Se, and Te within a complex multiphase spherical structure (raw slime sample 3, +C5 fraction). Brighter domains, in which up to ~ 12 wt% Au are measured by EDS spot analyses, lie within a grey Ag-Se-(Te) phase.

component of all slime samples by volume (Fig. 5). Measured compositions vary from sample to sample and semi-quantitative EDS compositional data are impacted by the presence of ubiquitous ultrafine inclusions. There are significant difference between compositions of the raw and decopperised/pH-neutralised samples. The 'matrix' component of raw slimes (Fig. 5A, B) contains 30–40 wt wt.% Cu, 4–12 wt% As, up to 3 wt% Ag, 5–10 wt% Se, and 1–2 wt% Te. Lead contents are < 1 %, and Sb contents anywhere from < 0.5 to ~ 5 wt% (quantitative electron probe data, also indicating H_2O contents of 20–30 %). Although most of the copper in raw slimes is contained within the colloidal matrix phase, we note subordinate copper as heavily corroded fragments of anode that separated and fell into the slimes tank.

In the decopperised (Fig. 5C-E) and pH-neutralised (Fig. 5F) samples, the 'matrix' phase hosts what still remains of Cu (typically 1–3 % Cu) and significant amounts of both Pb and Te (both consistently 5–9 wt%) alongside Bi (8–12 wt%), Sb (17–30 wt%) and As (4–7 wt%). Silver and Se concentrations in the colloidal matrix vary from < mdl to as much as ~ 8 wt%, although the higher-end values are most likely attributable to sub-micron-scale inclusions. Gold concentrations are erratic in 'matrix' from all samples but are generally lower in decopperised slimes, suggesting stabilisation of Au into selenides as shown in Fig. 3D.

The major compositional changes during decopperisation of matrix results from dissolution of Cu, As, Sb, Pb, and other elements from the raw slimes as acid is added. Whereas Cu and As are retained in electrolyte, Sb and Pb are reprecipitated to form a largely new colloidal 'matrix', dramatically modifying the Sb/As ratio. Silver, Au and Se are precipitated as 'new' phases, although some Ag-selenides appear to replace pre-existing Cu-selenides. We can also assume significant remobilisation of Te into the 'matrix' as the Cu-selenides are dissolved.

5.3. *$BiAsO_4$ and other Bi-As-Sb-(Sn) compounds*

A conspicuous feature of all samples (raw, decopperised and pH-neutralised) are relatively coarse fragments, some of which display a pronounced banded or layered structure suggestive of 'sedimentary' precipitation at the bottom of the refinery tank (Fig. 2C). Although many

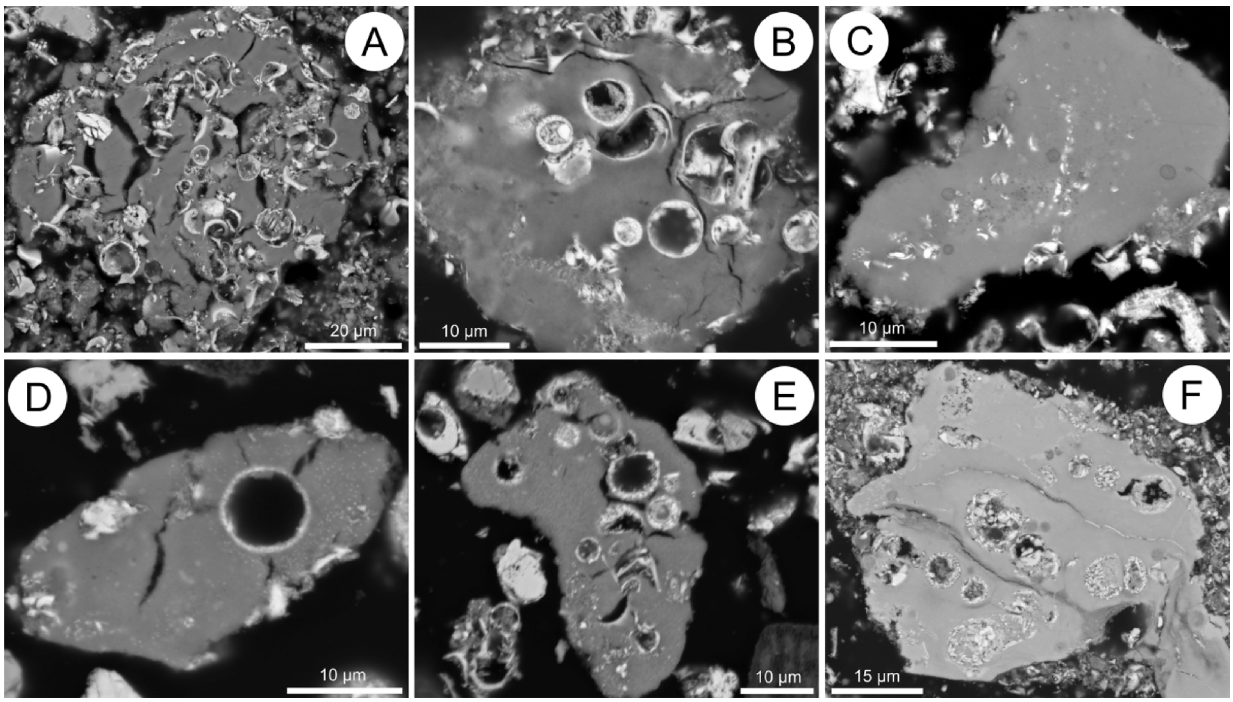

Fig. 5. BSE images showing aspects of colloidal matrix in raw (A and B), decopperised (C-E) and pH-neutralised slimes (F). (A) Typical appearance of colloidal matrix in raw slimes with dense spheroidal structures. (B) Higher-magnification images of compositionally inhomogeneous matrix containing filled and empty spheroidal structures. (C) Heterogeneous Sb-rich matrix in decopperised slimes with less abundant, largely decomposed spheroidal structures. (D and E) Sb-dominant matrix in decopperised slimes; note that larger spherical structure are now empty with fill mostly dissolved away. (F) Matrix fragment in pH-neutralised slime; note that most spherical structures are now decomposed.

of these fragments also contain minor amounts of sulphates (and Al-Sb-phases in some cases), BSE imaging reveals three main components: $BiAsO_4$ (usually with a few wt.% Sb), comparable with that described above from the spheroidal structures, Bi-Sb-(As)-oxide, and a markedly darker Sn-bearing Bi-Sb-As-oxide phase. The three phases are readily distinguished on BSE images (Fig. 6A). $BiAsO_4$ occurs as relatively thick bands, often forming the margins of the coarser fragments but also interlayered with Bi-Sb-(As)-oxides. Veins and thin seams of $BiAsO_4$ often penetrate entire fragments. $BiAsO_4$ can be semi-massive, but it also forms idiomorphic crystals growing into voids (Fig. 6B). Sometimes, it appears that $BiAsO_4$ replaces Bi-Sb-(As)-oxides, but other cases are more suggestive of Bi-Sb-(As)-oxide overgrowth on $BiAsO_4$ (Fig. 6C). The $BiAsO_4$ phase has a remarkably consistent composition irrespective of morphology, including when occurring as prismatic crystals (Fig. 6D), although with modest variations in Sb content from grain to grain, while maintaining the Bi:(As + Sb) ratio, and occasionally, visible compositional zoning with respect to Sb. It contains no measurable Ag, Se, or Te. Trace Cu (rarely as high as 1 % in raw slimes) is noted, as is SO_3 (typically < 0.5 % but up to 3.5 %). Sensitivity under the microprobe beam and relatively low analytical totals (94–96 %) prompted the nanoscale study documented in section 5.6 below to confirm the identity of the $BiAsO_4$ phase.

The Bi-Sb-(As)-oxide in the larger fragments contains 30–36 % Sb, 17–20 % Bi, 4–7 % As, with minor Pb, Sn, Cu and S. Unlike $BiAsO_4$, the Bi-Sb-(As)-oxide contains a couple of wt.% TeO_2. The darker layers on BSE images of the fragments are intimately intergrown with both the Bi-As-(Sb)- and Bi-Sb-(As)-oxides and contain around 16–22 wt% SnO_2, together with 15–25 % Sb_2O_3, 8–13 % Bi_2O_3, and 28–38 % As_2O_5. This compound appears to account for almost all Sn in the samples, appears largely unchanged across the three samples, suggesting it is stable during successive treatment.

Alongside the above compounds, we observe a morphologically diverse sub-group of Sb-dominant phases with broadly similar compositions that also contain several wt.% Pb and/or Te, and 1–2 wt% Sn. Although also observed in raw slimes, these 'phases' are most commonly encountered in decopperised and pH-neutralised slimes. They typically feature distinctive elongate or curved arrays of pores (Fig. 7) suggestive of formation as a viscous colloidal mush. EBSD analysis has shown they are non-crystalline.

5.4. Other components of slimes

The samples contain an eclectic group of phases derived from added scrap, resulting from acid treatment, or of technogenic derivation. These are concentrated in the coarsest size fractions and includes corroded fragments of pure copper metal in raw slimes that separated from dissolving anode, sulphates of Ba (baryte, $BaSO_4$), Pb (anglesite, $PbSO_4$) and a wide range of other Al-bearing compounds. Complex textures between Al-oxides and baryte result from the use of anode mould washes, in which anode moulds are coated with Al-oxides and barium sulphate prior to pouring the molten copper into the moulds. We also observe a number of silicate minerals probably originating from impurities in mould washes during anode casting.

5.5. Preliminary assessment of phase crystallinity

EBSD was applied to representative particles from all the above groups in a representative sample of raw slimes to obtain an indication of crystallinity in each compositionally distinct component. This work established that the ring- and atoll-like phases (section 5.1. above) are largely crystalline but that their infill, where present, is mostly glassy. Diffractions could be indexed as selenide minerals such as eucairite. The 'matrix' enclosing the ring- and atoll-like phases (Fig. 5) and the major component of the samples was found to be always amorphous, never revealing Kikuchi bands indicative of a crystalline structure. Thirdly, the $BiAsO_4$ phase (Fig. 6) is confirmed as crystalline, irrespective of whether it displays acicular habit, is observed growing into voids, or occurs as fine-grained aggregates within banded particles (Fig. 8). $BiAsO_4$ is

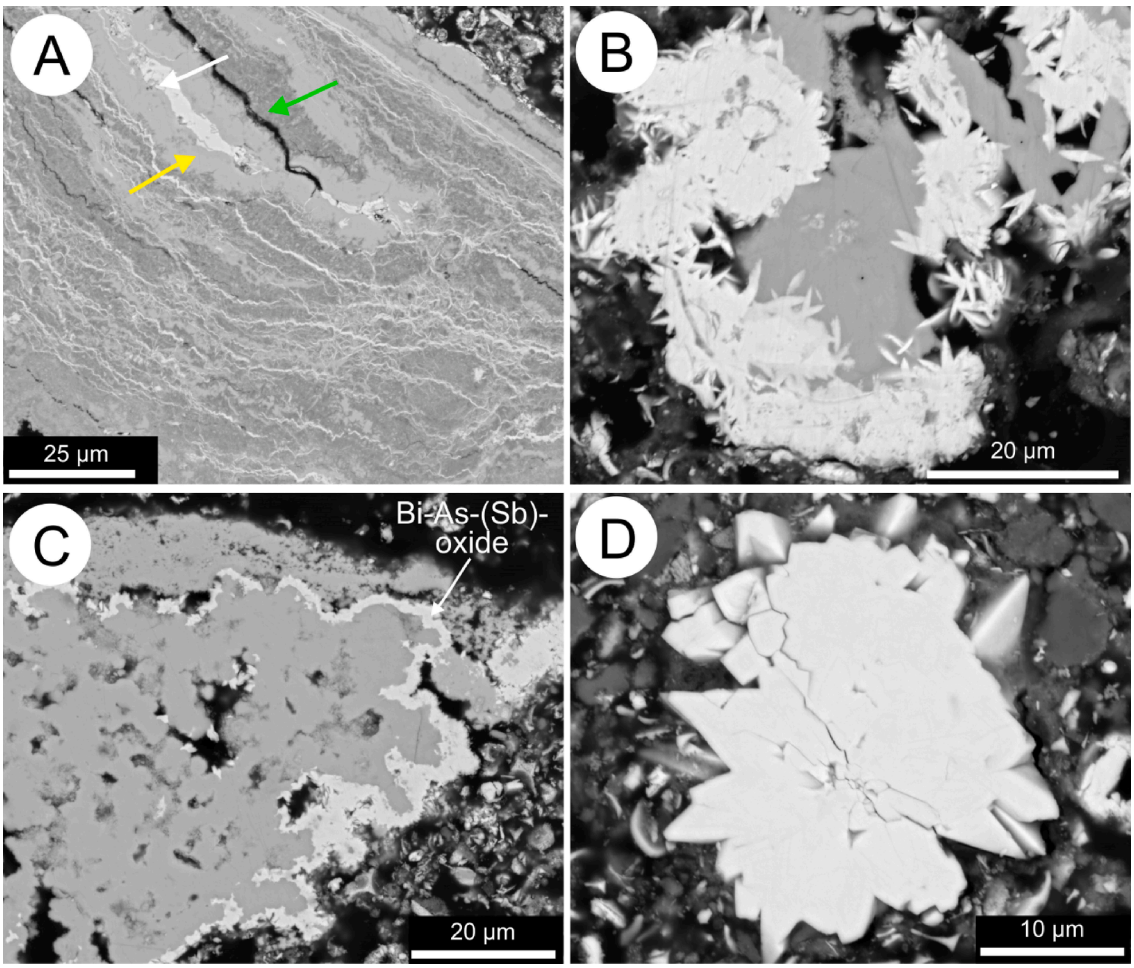

Fig. 6. BSE images showing aspects of Bi-As-Sb-oxide phases (A) Detail of larger, banded fragment in pH-neutralised slime showing three distinct components: $BiAsO_4$ as coarser patches and penetrating 'veins' appearing brightest on the image (white arrow); Bi-Sb-(As)-oxide (medium grey, yellow arrow) and Bi-Sn-Sb-(As)-oxide (darkest, green arrow). (B) Acicular needles of $BiAsO_4$ (bright) overgrowing fragment of Cu-As-dominant 'matrix' (medium grey, raw slime sample). (C) Overgrowth of $BiAsO_4$ at margin of partially crystalline (?) Sb-Bi-oxide (decopperised slime sample). (D) Prismatic $BiAsO_4$ (raw slime; 57 wt% Bi, 20 wt% As, 19 wt% O, 2 wt% Cu, 2 wt% Sb, normalised EDS data). (For interpretation of the references to colour in this figure legend, the reader is referred to the web version of this article.)

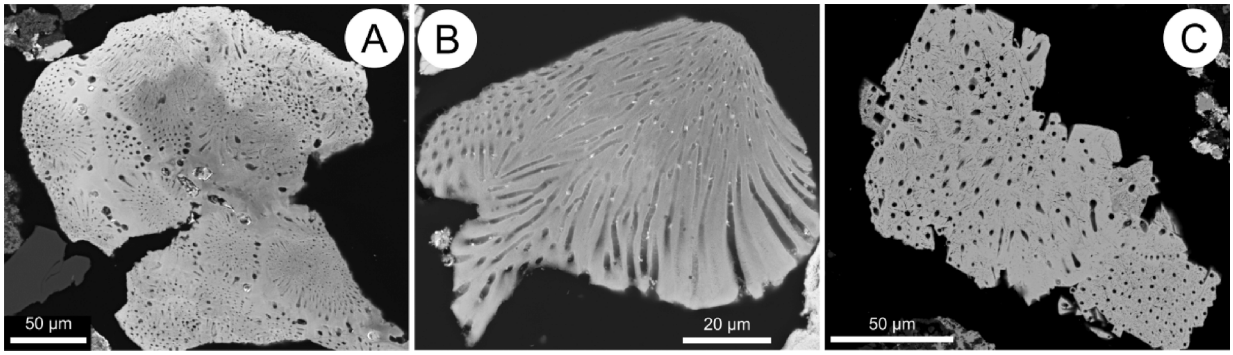

Fig. 7. BSE images showing examples of amorphous Sb-Bi-(Te) "phases" with characteristic elongate or curved pores observed in decopperised and pH-neutralised slimes. The phase in (C), from decopperised slime, yields 42 wt% Sb_2O_3, 20 wt% Bi_2O_3, 9 wt% TeO_2, 5 wt% As_2O_5, 3 wt% PbO, 2 wt% Cu_2O, and 1 wt% SnO_2, for an analytical total of ~ 82 %; electron probe data. Images A and B are from pH-neutralised slime with comparable compositions.

shown to be polycrystalline and could be indexed as three distinct minerals: anhydrous $BiAsO_4$, i.e., rooseveltite; and the hydrated Bi-As-oxides preisingerite, $Bi_3(AsO_4)_2O(OH)$, and atelestite, $Bi_2(AsO_4)O(OH)$. From these phases, rooseveltite consistently displayed the lowest mean angular deviation (Fig. 8D). In contrast, the associated Bi-Sb-oxide phases, including where they host $BiAsO_4$, are overwhelmingly non-crystalline, although some visibly granular Bi-Sb-oxide aggregates did give indications of incipient crystallinity.

5.6. Crystal structure of $BiAsO_4$

Identification of the $BiAsO_4$ phase from imaging, microprobe

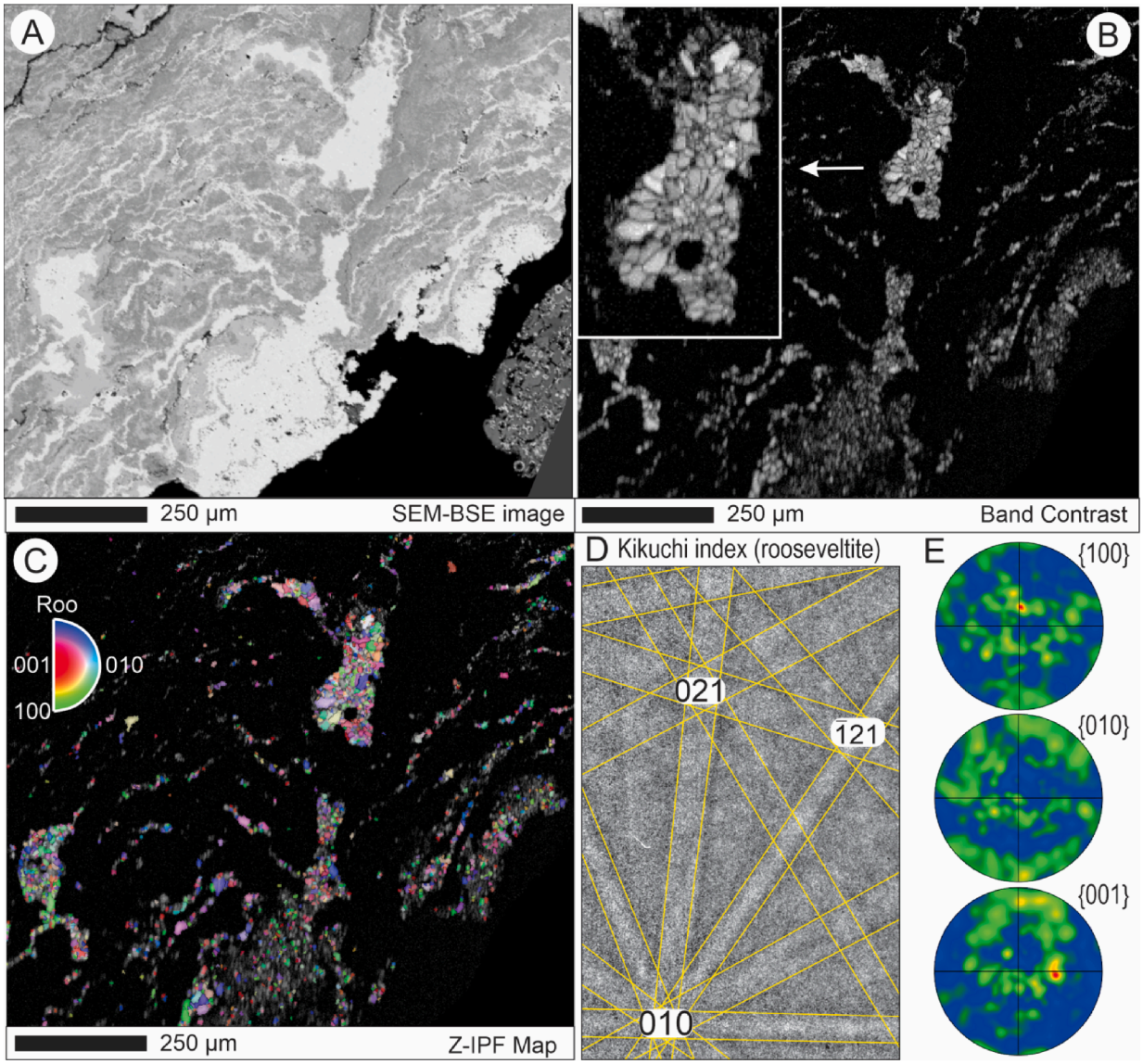

Fig. 8. (A) BSE image of the $BiAsO_4$ phase (bright) and associated Bi-Sb-(Sn)-oxide (grey). EBSD band contrast map (B) and Z-inverse pole figure (IPF) map (C) show that the $BiAsO_4$ phase is crystalline and composed of a fine aggregate (emphasised on the band contrast enlargement given as an inset on C), whereas the enclosing Bi-Sb-(Sn)-oxide matrix is amorphous. The crystalline phase was indexed as rooseveltite on Aztec EBSD software (D) with the corresponding pole figures displaying orientations of analysed crystalline grains.

analysis and EBSD alone proved equivocal. There are two named minerals with composition $Bi(AsO_4)$: α-$Bi(AsO_4)$, rooseveltite (monoclinic); and β-$Bi(AsO_4)$, tetrarooseveltite (tetragonal) (Mooney, 1948; Bedlivy and Mereiter, 1982a; Sejkora and Řídkošil, 1994). There are two named hydroxlated species: atelestite, $Bi_2(AsO_4)O(OH)$ (Mereiter and Preisinger, 1986); and preisingerite, $Bi_3(AsO_4)_2O(OH)$ (Bedlivy and Mereiter, 1982b). The measured stoichiometry, clearly indicating a Bi/(As + Sb) ratio of ~ 1 matches neither of these yet the low totals and beam sensitivity led us to suspect a degree of hydration.

Given this uncertainty, we undertook a nanoscale study on a thinned foil cut and extracted from a representative cluster of acicular $BiAsO_4$ crystals (Fig. 9A, B). We believe this to be the first attempt to resolve crystal structure in refinery slimes using scanning electron transmission microscopy. EDS nanoscale mapping across the boundary between $BiAsO_4$ and the amorphous Sb-As-Bi-oxide host confirmed phase chemistry (Fig. 9C). Atomic-scale imaging on three different zone axes, electron diffraction and comparison with STEM simulations (Fig. 9D) confirm the identity as α-$Bi(AsO_4)$, i.e., rooseveltite. We note, however, a slight divergence between the structure of the chemical precipitate in the slimes and the defined mineral that may be linked to rate of crystallisation; we cannot rule out a limited degree of hydration.

6. Discussion

6.1. Element deportment and evolution during subsequent processing

Fig. 10 is a schematic outlining slime composition/mineralogy and a heavily simplified evolution of impurity element deportment from their occurrence in anode (Cook et al., in review) through dissolution, followed by raw slime precipitation, subsequent decopperisation, to pH-neutralisation.

In raw slimes from Olympic Dam, silver is primarily found within a ~ AgCu(Se,Te) phase and within the colloidal matrix (possibly as ultrafine inclusions?). Upon decopperisation and in pH-neutralised samples, Ag becomes almost exclusively present in the form of Ag-selenide (~Ag_2Se), although we observe survival of some Cu-Ag-selenides. Silver deportment in slimes and behaviour during electrorefining is thus intimately linked to that of Se. Scott (1990) discusses the importance of

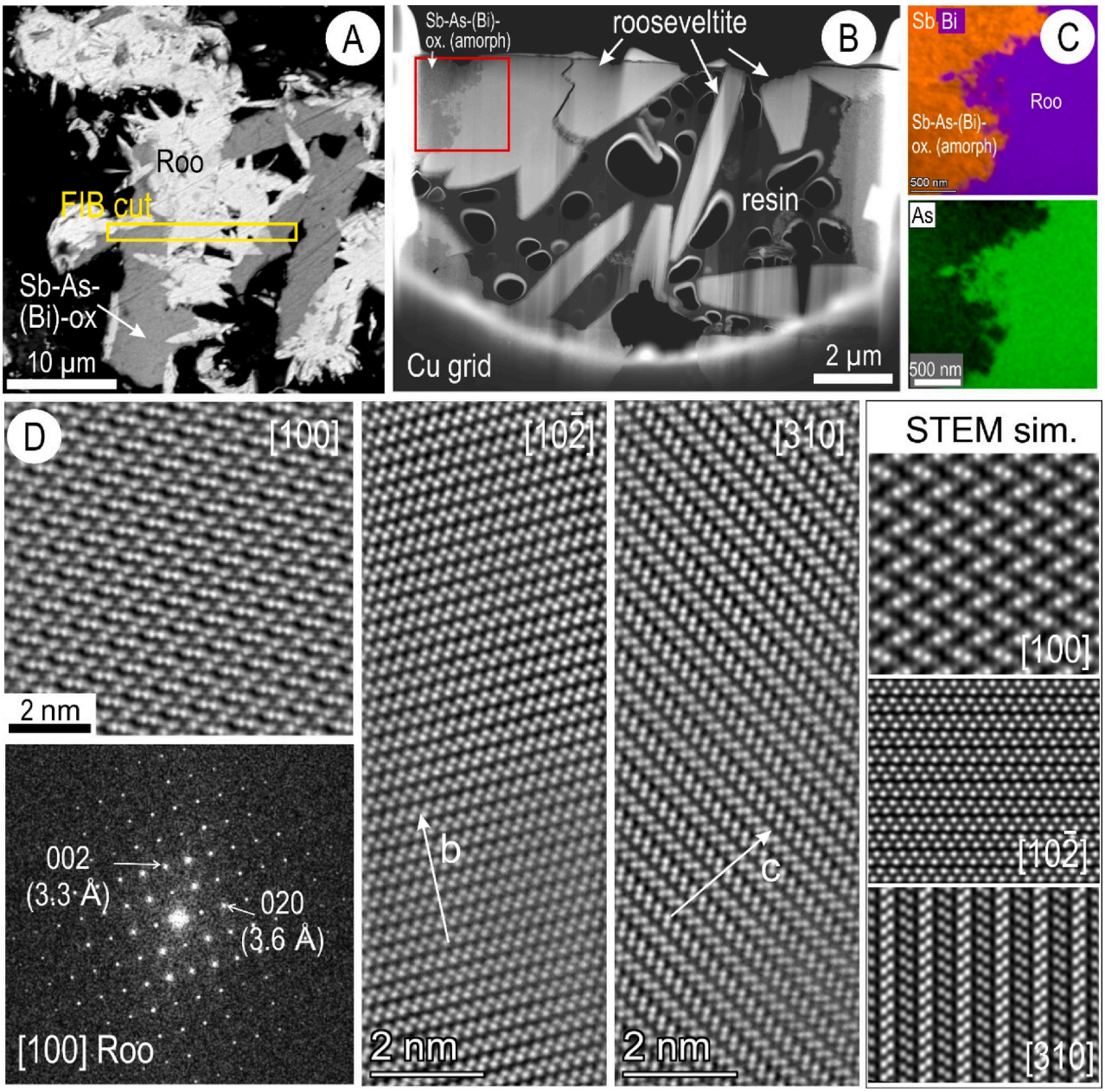

Fig. 9. (A) BSE image showing grain(s) selected for nanoscale study and location of FIB cut. (B) View of thinned foil. Note acicular $BiAsO_4$ growing into void (now resin) and associated amorphous Sb-As-Bi phase. (C) EDS element maps of boundary area between $BiAsO_4$ and amorphous Sb-As-Bi phase indicated by red box on B. (D) Atomic-scale HAADF STEM images for three zone axes as marked by notation in square brackets. Note excellent correspondence with STEM simulations for the same zone axes shown at right. Fast Fourier transform pattern on [1 0 0] zone axis (lower left) confirms identification of the phase as α-$BiAsO_4$ (rooseveltite, Roo). (For interpretation of the references to colour in this figure legend, the reader is referred to the web version of this article.)

the Ag:Se molar ratio in anode and how that might be used to predict slime mineralogy, also noting the same "superstoichiometric" composition of Cu-selenide inclusions in copper anode that we have identified (Cook et al., in review). Chen and Dutrizac (1989a) discuss evidence for reaction between Ag^+ in electrolyte (from dissolution of solid solution silver in anode copper) and Cu-selenide inclusions in the anode that have not dissolved. This can lead to variation in stoichiometry, even within single AgCu(Se,Te) particles, a phenomena also noted by us. Chen and Dutrizac (1989a) stress the point that conditions in commercial refinery operations do not necessarily allow for complete equilibration, meaning that the residence time of liberated Cu-selenide in electrolyte plays a role, and that there may be a stratification of compositions and diversity of species within the tank, e.g., Ag-rich species concentrate at the bottom of the cell.

Present data show that gold occurs in solid solution within Cu-Ag- and Ag-selenides at concentrations of up to a couple of wt.%, and as discrete microgranular inclusions of $Ag_3Au(Se,Te)_2$ within the selenides. These observations are consistent with published data (e.g., Chen and Dutrizac, 2004, 2008) and confirmation of phase stoichiometry from Mossbauer spectroscopy (Sawicki et al., 1993). No metallic gold or electrum (and only very minor metallic silver) was seen, an observation possibly explained by the relatively high Se and Te contents of Olympic Dam slimes compared to those from other plants. Additional discussion of the diversity of Cu-Ag-selenides and the nature of contained gold is beyond the scope of the present manuscript and requires empirical evidence from nanoscale studies.

Decopperisation modifies the distribution of Se, which is dissolved from the colloidal matrix and is redeposited as Ag-selenides. Indeed,

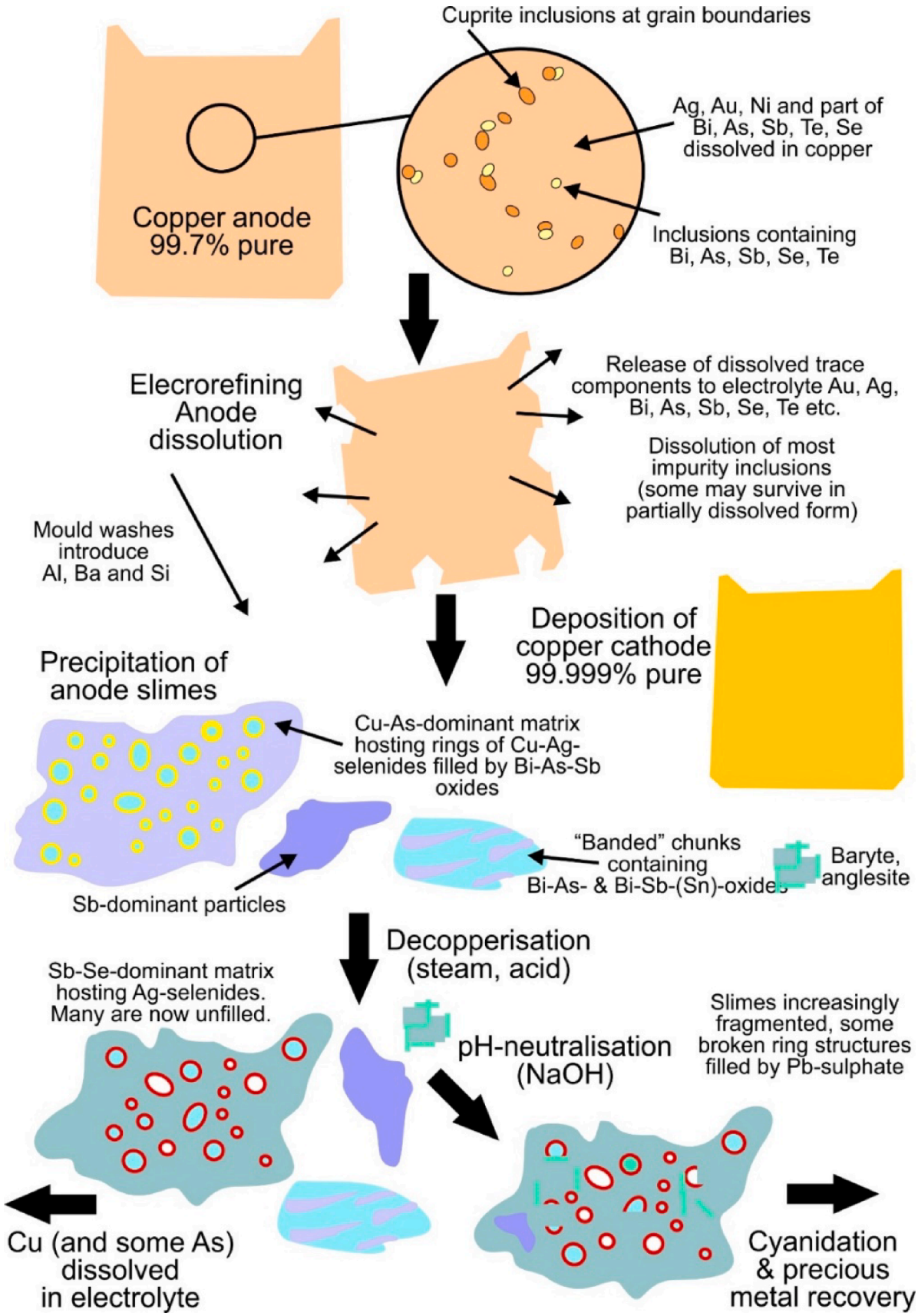

Fig. 10. Schematic diagram illustrating the evolution of impurity mineralogy from copper anode through dissolution, slime precipitation, decopperisation and pH-neutralisation. Note that for readability, the schematic is heavily simplified with only the main phases indicated. Compositions of all phase groups and data on low-abundance components will be described in detail elsewhere at a later date.

according to Ojebuoboh (2008), around 98 % of all Se precipitates into slimes and is insoluble in electrolyte. At first sight, tellurium would appear to closely follow Se, in that all selenide phases (Cu-, Cu-Ag- and Ag-selenides) also contain Te, concordant with published data, and that the Se/Te ratios in these phases are comparable to that in bulk slimes. However, measurable concentrations of Te are noted in the decopperised matrix yet not in the raw slime matrix, in direct contrast to Se, suggesting release and limited remobilisation of Te and, as would be expected during decopperisation, some dissolution of Te from the (Te-bearing) Cu-Ag-selenides. The different behaviours of Se and Te are linked to reaction kinetics and their relative capacities to combine with Cu and Ag. Chen and Dutrizac (1996) discuss the deportment of Te in raw anode slimes, noting that Te can be expected in the matrix (oxidate) in raw slimes, albeit as ultrafine-grained inclusions of discrete phases, which our analyses sought to avoid. These authors also mention Cu-Te oxide, which was not observed in our samples.

Unlike Se, Te, or Pb, which report almost exclusively to slimes, As, Sb, and Bi are soluble and thus partitioned between electrolyte and slimes depending on their concentrations (Chen and Dutrizac, 1990). A significant proportion of the total As in raw slimes from Olympic Dam occurs in the colloidal oxidative matrix (a feature of relatively low-As slimes; Moats et al., 2012), with the rest precipitated as $BiAsO_4$, identified here as rooseveltite. While the latter phase seems to be stable (or is readily reprecipitated), decopperisation dissolves virtually all As from the colloidal matrix. Rooseveltite is the main As-bearing phase in decopperised and pH-neutralised slimes.

In raw slimes, antimony occurs in a wide range of amorphous or poorly crystalline As-Sb oxide, As-Sb-Bi oxide and less common $SbAsO_4$ compounds. Species diversity may be linked to the different states of oxidation, Sb^{3+} and Sb^{5+} present (Beauchemin et al., 2008). Acid treatment during decopperisation dissolves a significant part of the Sb, which is subsequently reprecipitated in the colloidal matrix, as well as forming discrete Bi-Sb-oxide compounds, and as a subordinate component of Bi-As-(Sb)- and Bi-Sb-Sn-oxides.

Consistent with prior work (e.g., Moats et al., 2012), a major proportion of Bi in the relatively high-Bi Olympic Dam slimes occurs as rooseveltite whether infilling spherical structures or as a major component of the larger 'sediment-like' chunks. Thus, rooseveltite is the $BiAsO_4$ species that appears to be a stable phase throughout the process, also in agreement with published work from other copper refineries (e.g., Beauchemin et al., 2008). Subordinate amounts of Bi occur within the various Sb-bearing compounds and in the non-crystalline, Cu-bearing matrix hosting the atoll-like structures. The behaviour of bismuth during electrorefining is less well studied than that of As or Sb, largely attributable to its typically far lower concentration than in the Olympic Dam slimes. Dissolution of the matrix during decopperisation, releasing Bi and As, would explain the coatings of rooseveltite, veining and replacement of larger chunks and crystallisation of rosette-like rooseveltite crystals in pore spaces. Importantly, Bismuth does not form tellurides (or other chalcogenides) as it does under hydrothermal conditions, an observation linked to the oxidative environment, ready availability of As and Sb, and tank temperature well below the melting point of bismuth.

Lead precipitates as fine-grained $PbSO_4$ that occurs throughout the slimes. Lead would seem to re-dissolve during decopperisation, precipitating again as $PbSO_4$ but now also concentrated within the colloidal matrix (as ultrafine inclusions?), as well as infilling the atoll-like structures. Chen and Dutrizac (2003) show that complex Cu-Pb-As-Sb-Bi-oxide phases in copper anode, comparable with those documented from Olympic Dam (Cook et al., in review), dissolve only slowly or transform directly to a poorly soluble phase, which together with $PbSO_4$, continue to be associated with, and often fill the selenide spheroids. Chen and Dutrizac (2003) also argue that a high Pb content in anode will inhibit dissolution of Sb and Bi impurity inclusions which may pass directly into the slimes.

At Olympic Dam, tin is almost exclusively contained within a conspicuous Sn-As-Sb-oxide containing ~ 20 % wt.% Sn which occurs with $BiAsO_4$ and other Bi-Sb-(As)-oxides and is concentrated within the coarser 'banded' chunks. The Sn-bearing phase appears to precipitate early and remain stable through decopperisation and pH-neutralisation.

Although baryte and Al-bearing compounds largely represent a substrate for precipitation of other phases and are commonly observed at the centre of larger slime particles, some reaction with electrolyte is seen, notably the presence of the Ba-arsenate $Ba_3(AsO_4)_2$. Experimental evidence for sorption of arsenate (and to a lesser extent, selenate) onto the baryte surface at pH ~ 5 has recently been reported (Yang et al., 2023).

6.2. Comparison with element distributions in other refinery operations

Broadly the refinery operation at Olympic Dam resembles many other copper refineries globally. The slime compositions, phase assemblages, and the behaviour of individual elements reflect, however, the unique composition of source feedstock(s), the technologies used prior to electrorefining and the respective treatment conditions during concentration, leaching, smelting and anode casting. Direct comparison of characterisation studies from other refineries serves to emphasize the great diversity of possible phases and assemblages covering widely varying slime compositions (e.g. compilations of compositional data from various plants given by Cooper, 1990, Hait et al. (2009), Mastyugin and Naboichenko (2012), Xing et al. (2019) and Schlesinger et al. (2022).

In their study of high-Ni anode slimes from Inco's Copper Cliff refinery, Sudbury, Ontario, Canada, Chen and Dutrizac (1988a) note rapid reaction of Cu_2Se with electrolyte-borne Ag^+ to form AgCuSe and importantly for our work, a range of different stoichiometries among Cu-Ag-selenides, even with a single grain. The authors noted that although Te was mostly contained within the selenide, the telluride Ag_2Te may sometimes be precipitated during silver enrichment. This has not been observed in the Olympic Dam slimes, even though the bulk Se/Te ratios are broadly comparable in the two refineries.

In a later publication, Chen and Dutrizac (1993) examined mineralogical changes during decopperisation at the Kidd Creek refinery, Ontario, Canada. Although the contents of As, Sb, and Bi are far lower, and Pb far higher, raw slimes from Kidd Creek have similar contents of Cu, Ag and Se, and display some mineralogical commonalities with the Olympic Dam specimens. Similarities include the aberrant stoichiometry of Cu-Ag-selenides suggestive of intergrowths of two or more phases at the nanoscale and the presence of a Sn-arsenate phase that may be related to that described here. The decopperisation process is seen to dissolve some Te along with Cu, and lead to precipitation of Ag_2Se. Interestingly elemental selenium was reported by Chen and Dutrizac (1993) and attributed to H_2Se generation and subsequent oxidative precipitation of Se. The very minor elemental Se observed in similarly highly porous grains in Olympic Dam slimes (documented elsewhere; Cook et al., in review) may have a similar origin.

Chen and Dutrizac (1991) investigated anode slimes from Chuquicamata, Chile, that are somewhat similar to ours apart from significantly lower Bi. Similarities reported include the dominance of an agglomerated "oxidate" matrix phase (which the authors regard as a "complex Cu-Ag-arsenate-antimonate-selenite-sulphate-chloride", and the persistent presence of Te in the selenides. Notable is the description of Au as tiny inclusions within the selenides closely resembling those shown here. Other major differences include the relative presence of $CuSO_4{\cdot}5H_2O$, elemental silver, and silver chloride (chlorargyrite, AgCl). All three of these are observed in Olympic Dam slimes but only in very small amounts.

Controlling Group 5A elements in electrolyte is important for avoidance of "floating slimes", anode passivation, and prevention of trapping slime particles or electrolyte within cathode copper (Abe et al., 1980; Cheng and Hiskey, 1996; Moats et al., 2012). Floating slimes are generated by oxidation of Sb^{3+} in electrolyte to Sb^{5+}, a process linked to

As activity (Moats et al., 2012). Antimony behaviour is still relatively poorly constrained and appears heavily related to that of other components, notably As and Bi. Reactions among tri- and pentavalent forms of As and Sb include generation of arsenato antimonic acid and the subsequent precipitation of arsenato antimonates (Wang et al., 2006).

Chen and Dutrizac (2005) addressed high-Pb anode slimes from the La Caridad copper refinery, Mexico, observing species such as $Pb_5(AsO_4)_3(OH,Cl)$, Pb-Sb- and Pb-Bi-oxides, The authors argue that high Pb contents promote precipitation of "Sb-As-O species", reducing As and Sb concentration in electrolyte. At Olympic Dam, beside $PbSO_4$, Pb is present only as minor component of some Bi-As-Sb-oxides.

In a more recent study, Aguilera et al. (2015) describe raw and decopperised slimes from "a Chilean refinery". In raw slimes containing Au, Ag, Cu, As, Se, Te and PGM, the authors identified CuAgSe, Ag_2Se, $SbAsO_4$ and $PbSO_4$. The authors report and illustrate various phases, including crystalline $SbAsO_4$, $Ag_{2-x}Se$, and chlorargyrite in decopperised slimes. These findings include some of the phases documented here from Olympic Dam, but the presence of significant Bi and minor Sn at Olympic Dam highlight the impact of differences in feed ore and the role this has for phase speciation and textures in the slimes.

6.3. Recovery options and economic considerations

BHP Olympic Dam currently sends neutralised slimes for cyanidation to recover gold and silver. Annual gold and silver production were 138,400 oz and 743,000 oz in the 2022 financial year.

Globally, around 90 % of Te is sourced from reprocessing anode slimes from copper electrorefineries, with the balance recovered as a by-product of lead, zinc and gold mining (Ojebuoboh, 2008). There exists latent potential for expanded production from refinery slimes, given that annual global Te production is only around one quarter of the total Te contained in slimes generated worldwide (Nassar et al., 2022). The rise of tellurium, a critical mineral used in the production of solar panels and other photovoltaics has seen annual demand double over the last 10 years and demand is predicted to rise three-fold by 2050 (USGS, 2014). This has led some major copper producers to add Te recovery streams to existing copper operations, notably by Rio Tinto at its Kennecott copper mine in Utah (Rio Tinto, 2022), who plan 20 tonnes Te production annually. Different options exist to recover Te from refinery slimes and other metallurgical wastes (e.g., Mahmoudi et al., 2020; Li et al., 2022), as well as for Se (e.g., Wang et al., 2016).

There is no recovery of Te from slimes at Olympic Dam at the present time and no current plans to recover Te or other metals. This situation is unlikely to change in the foreseeable future. The main reason that Te and Se recovery is not attempted lies with the significant concentrations of ^{210}Pb and ^{210}Po in Olympic Dam slimes, even though the volumes are small (Appendix S to BHP, 2009). Secondly, although the deposit represents a global Te anomaly, the element represents a low-volume, relatively low-value by-product that is insignificant on the scale of the existing operation. To be viable, Te recovery would need to be inexpensive and not impair or reduce recovery of the four revenue metals (copper, uranium, gold, and silver). Recovery of a clean saleable concentrate would be required. The market price for Te at the time of writing (22 June 2023) is ~ USD 80/kg, i.e., just above 1 % of the gold price (~USD 1900/oz), and little more than one-tenth of the silver price (~USD 22/oz). Similar considerations apply to Sb, Bi, and Se that are even less valuable (all currently around USD 12 and 20 per kg).

In slimes, Sb, Bi and Sn occur mainly as oxides, in contrast to As which mainly exists as arsenate. A range of technologies exist for removal or recovery of arsenic, antimony, bismuth, and tin from refinery slimes. Zeng et al. (2023) propose compound leaching and subsequent precipitation of oxychlorides. Similarly, Sb and Bi can be removed from electrolyte using activated carbon or ion-exchange resins (Ando and Tsuchida, 1997; Navarro and Alguacil, 2002; Arroyo-Torralvo et al., 2017; Artzer et al., 2018). Industrial implementation of Sb and Bi removal technologies in the Atlantic Copper Refinery (Huelva, Spain) have been shown to contribute to mitigation of floating slimes and pipe scale formation (González de las Torres et al., 2021). Most recently, Luo et al. (2023) have demonstrated a selective precipitation process to control Sb and Bi and potentially recover both elements from slimes.

Moats et al. (2021) have estimated that the copper anodes produced globally each year contain 7,900 tonnes Se, 2,300 tonnes Te, 24,000 tonnes As, 7,100 tonnes Sb, and 5,100 tonnes Bi. Such volumes, particularly of Se and Te, could significantly boost current world production of these sought-after elements. Technological innovation will be required to achieve economic recovery and in complex, polymetallic slimes like Olympic Dam, to enable efficient recovery of one element without hampering the extraction of another. Enhanced collaboration and sharing of expertise between corporate entities, potentially pooling slimes, electrolytes and smelter dusts, and sharing recovery facilities, could also be significant for increased recovery of these minor elements as by-products of the primary copper supply chain.

7. Conclusions and implications

Seven main conclusions can be drawn from this study:

1. Comprehensive assaying of different batches of anode slimes from Olympic Dam shows that their bulk compositions vary and that each size fraction can have a markedly different concentrations of key elements. Gold, Ag, Pb, Se and Te are all preferentially enriched in the –C5 fraction, whereas Bi, Sb, Sn Si, and Al are highest in the coarse fractions.
2. Decopperisation of raw slimes by acid addition results in the loss of about one-third of the material (from ~ 30 % to < 1 % Cu) to electrolyte, giving an ostensible increase in the concentrations of most other elements. Arsenic concentration drops in absolute terms, by around half, during copper removal. Relatively little Sb or Bi remains dissolved and is immediately re-precipitated.
3. Slimes contain four broad groups of component "phases': (i) micron-sized spherical, ring- and atoll-like structures dominated by Cu-Ag- and Ag-selenides and infilled, in part, by Bi-As-(Sb)-oxides; (ii) amorphous, compositionally variable Cu-As-dominant 'matrix' hosting the ring- and atoll-like structures in raw slimes, giving way to a Sb-Se-bearing matrix following decopperisation; (iii) crystalline $BiAsO_4$, amorphous Bi-Sb-oxides and other As-, Sb- and Sn-bearing compounds; and (iv) various sulphates, alloys, silicates, and Al-bearing phases.
4. Decopperisation leads to dissolution of As-bearing phases, leaving voids, but also resulting in some replacement and redistribution of Sb, Se and Te. Decopperised and pH-neutralised samples appear less crystalline, with phases either decomposed or visible heterogeneous at the micron-scale or below. Selenides are commonly intergrown with sulphates, notably $PbSO_4$, the dominant Pb-bearing phase in all samples.
5. Tellurium-bearing Cu-Ag-selenides are the main host for Ag, Se, and Te in the raw slimes but are largely replaced by Ag-selenides (that also contain Te) in decopperised slimes. Gold occurs dissolved within the Cu-Ag- and Ag-selenides but also as microgranular inclusions of a discrete $Ag_3Au(Se,Te)_2$ phase.
6. HAADF STEM study of the $BiAsO_4$ phase has confirmed its identity as α-$BiAsO_4$, corresponding to the mineral rooseveltite. This is one of the few crystalline phases that remains stable from initial precipitation through decopperisation and pH-neutralisation, consistent with published work on slimes from other refineries.
7. Precious metals are recovered from Olympic Dam slimes by cyanidation, but by-product recovery of Te, Sb, or other metals is not deemed economic at the present time.

Several implications can be drawn from this work. Firstly, the empirical data needed to resolve outstanding research gaps in slimes characterisation can be obtained, at least in part, by the application of

complementary state-of-the-art microanalytical and imaging techniques widely used in mineralogy and materials science. These include EBSD and STEM as used here but could also involve others such as Raman spectroscopy. Application of these techniques to suitable study cases, considering both speciation and textures is likely to expand rapidly as demand for detailed information to underpin innovation in extractive metallurgy increases. Importantly, these techniques have a role to play in the characterisation of a a range of other materials, including tailings in long-term storage and historical smelter slags.

Characterisation of slimes presents challenges in terms of fine particle size, abundant (non–)crystallinity, sensitivity to the electron beam, non-stoichiometry, and the abundance of ultrafine mixtures and intergrowths. With some obvious exceptions (e.g., baryte, anglesite), giving mineral names to phases based solely on chemistry and without determination of crystal structure may be misleading.

Although phase assemblages in anode slimes from Olympic Dam are comparable with those described from other refinery operations worldwide, the diversity of textures and species in a slime and their compositions reflects the diversity of ore assemblages and their relative enrichment in many minor elements. Metallurgical considerations cannot therefore ignore the importance of ore geology, mineralogy, and textures.

Reactions in refinery slimes are complex, often interdependent with one another, and may often not attain equilibrium. Although significant progress has been made in the past 30 years to develop models of element deportment for electrorefinery slimes that have generic application, several aspects of slime mineralogy remain poorly constrained. These include how the relative abundances of As, Sb, Bi and Pb in anode govern partitioning between slime and electrolyte and the species present in slimes, and the crystal-chemical character of the Cu-Ag, Ag-, and Ag-Au-selenide phases.

Olympic Dam refinery slimes are well suited to further study in that they contain moderate to high concentrations of all key elements (Bi, Sb, Te, Se, Sn, and Pb). With this in mind, we have embarked on a further high-resolution transmission electron microscopy investigation of crystal structures present in Cu-selenide (anode) and the Ag-Cu- and Ag-selenides (slimes), and their relationships with known species in the systems Ag-Se, Ag-Se-Te, and Cu-Ag-Se.

Author contributions

K.E. and N.J.C. conceived this research. K.E. and V.L. provided samples, extensive insight and guidance. Imaging and microanalysis work was conducted by N.J.C. C.L.C. assisted with interpretation and data presentation. S.A.K. performed the EBSD analyses. A.S. assisted with the HAADF STEM study. The manuscript was written by N.J.C., C.L.C. and K.E.

CRediT authorship contribution statement

Nigel J. Cook: . **Kathy Ehrig:** . **Cristiana L. Ciobanu:** Conceptualization, Investigation, Methodology, Writing – original draft, Writing – review & editing. **Samuel A. King:** . **Vanessa Liebezeit:** Resources, Validation, Writing – original draft. **Ashley D. Slattery:** Formal analysis, Investigation, Writing – original draft.

Declaration of competing interest

The authors declare that they have no known competing financial interests or personal relationships that could have appeared to influence the work reported in this paper.

Data availability

Data will be made available on request.

Acknowledgements

This is a contribution to the Australian Research Council Linkage Project LP200100156 (Critical Metals from Complex Copper Ores) co-supported by BHP Olympic Dam. We appreciate comments from three anonymous reviewers and sincerely thank Editor Anna Kaksonen for her handling of this manuscript.

References

Abe, S., Burrows, B.W., Ettel, V., 1980. Anode Passivation in Copper Refining. Can. Metall. q. 19, 289–296.
Aguilera, E.M., Hernández, M.C., Viñals, J., Seguel, T.G., 2015. Characterization of raw and decopperized anode slimes from a Chilean refinery. Metall. Mater. Trans. B 47, 1315–1324.
Ando, K., Tsuchida, N., 1997. Recovering Bi and Sb from electrolyte in copper electrorefining. JOM 49, 49–51.
Arroyo-Torralvo, F., Rodríguez-Almansa, A., Ruiz, I., González, I., Ríos, G., Fernández-Pereira, C., Vilches-Arenas, L.F., 2017. Optimizing operating conditions in an ion-exchange column treatment applied to the removal of Sb and Bi impurities from an electrolyte of a copper electro-refining plant. Hydrometall. 171, 285–297.
Artzer, A., Moats, M., Bender, J., 2018. Removal of Antimony and Bismuth from Copper Electrorefining Electrolyte: Part I—A Review. JOM 70, 2033–2040.
Beauchemin, S., Chen, T.T., Dutrizac, D., 2008. Behaviour of antimony and bismuth in copper electrorefining circuits. Can. Metall. q. 47, 9–26.
Bedlivy, D., Mereiter, K., 1982a. Structure of alpha-$BiAsO_4$ (rooseveltite). Acta Cryst B38, 1559–1561.
Bedlivy, D., Mereiter, K., 1982b. Preisingerite, $Bi_3O(OH)(AsO_4)_2$, a new species from San Juan Province, Argentina: Its description and crystal structure Am. Mineral. 67, 833–840.
BHP Billiton, 2009 Olympic Dam Expansion. Draft Environmental Impact Statement 2009. 2. Existing Operation. www.bhp.com.
Chen, T.T., Dutrizac, J.E., 1987 The Electrorefining and Winning of Copper. In: J.E. Hoffman, R.G. Bautista, V.A. Ettel, W.R. Kudryk (eds.), Symposium Proc., TMS 116th Annual Meeting, Denver, CO, Feb. 24-26th 1987), p. 499-525.
Chen, T.T., Dutrizac, J.E., 1993 Mineralogical changes occurring during the decopperizing and deleading of Kidd Creek copper refinery anode slimes. In: Extractive Metallurgy of Copper, Nickel and Cobalt, Volume 1: Fundamental Aspects (R.G. Reddy, R.N. Weizenbach, eds.), The Minerals, Metals & Materials Society, Warrendale, PA, p. 337-401.
Chen, T.T., Dutrizac, J.E., 1988a. Mineralogical characterization of anode slimes—II. Raw Anode Slimes from Inco's Copper Cliff Copper Refinery. Can. Metall. q. 27, 97–105.
Chen, T.T., Dutrizac, J.E., 1988b. Application of Electron Microscopy to the Electrorefining of Copper. Scanning Microsc. 2, 735–746.
Chen, T.T., Dutrizac, J.E., 1989a. Mineralogical characterization of anode slimes—IV. Copper-Nickel-Antimony Oxide ("Kupferglimmer") in CCR Anodes and Anode Slimes. Can. Metall. q. 28, 127–134.
Chen, T.T., Dutrizac, J.E., 1989b. A mineralogical study of the deportment and reaction of silver during copper electrorefining. Metall. Mater. Trans. B 20, 345–361.
Chen, T.T., Dutrizac, J.E., 1989c. The mineralogy of copper electrorefining. JOM 42, 39–44.
Chen, T.T., Dutrizac, J.E., 1990. Mineralogical characterization of anode slimes: Part 6—Pressure leached slimes from the CCR Division of Noranda Minerals Inc. Can. Metall. q. 29, 293–305.
Chen, T.T., Dutrizac, J.E., 1991. Mineralogical Characterization of Anode Slimes: Part 7—Copper Anodes and Anode Slimes from the Chuquicamata Division of Codelco-Chile. Can. Metall. q. 30, 95–106.
Chen, T.T., Dutrizac, J.E., 1996. Mineralogical characterization of anode slimes: Part 10. Tellurium in raw anode slimes. Can. Metall. q. 35, 337–351.
Chen, T.T., Dutrizac, J.E., 2003. A mineralogical study of the effect of the lead content of copper anodes on the dissolution of arsenic, antimony and bismuth during copper electrorefining. Can. Metall. q. 42, 421–432.
Chen, T.T., Dutrizac, J.E., 2004. Gold in the electrorefining of copper and the decopperizing of copper anode slimes. JOM 56, 48–52.
Chen, T.T., Dutrizac, J.E., 2005. Mineralogical characterization of a copper anode and the anode slimes from the La Caridad copper refinery of Mexicana de Cobre. Metall. Mater. Trans. B 36, 229–240.
Chen, T.T., Dutrizac, J.E., 2008. Mineralogical overview of the behavior of gold in conventional copper electrorefinery anode slimes processing circuits. Mining. Metall. Explor. 25, 156–164.
Cheng, X., Hiskey, J.B., 1996. Fundamental studies of copper anode passivation during electrorefining: Part I. development of techniques. Metall. Mater. Trans. B 27, 393–398.
Cook, N.J., Ehrig, K., Ciobanu, C.L., Gilbert, S., in review. Impurity components in anode copper from Olympic Dam, South Australia. Minerals Engineering.
Cooper, W.C., 1990. The treatment of copper refinery anode slimes. JOM 42, 45–49.
Ehrig, K., McPhie, J., Kamenetsky, V.S., 2012 Geology and mineralogical zonation of the Olympic Dam iron oxide Cu-U-Au-Ag deposit, South Australia. In Geology and Genesis of Major Copper Deposits and Districts of the World, a Tribute to Richard Sillitoe; Hedenquist, J.W., Harris, M., Camus, F., Eds.; Soc. Econ. Geol.: Littleton, CO, USA, p. 237–268.

Ehrig, K., Kamenetsky, V., McPhie, J., Cook, N.J., Ciobanu, C.L., 2017. Olympic Dam iron-oxide Cu-U-Au-Ag deposit. In: Phillips, G.N. (Ed.), Australian Ore Deposits. AusIMM, Melbourne, pp. 601–610.

González de las Torres, A.I., Moats, M.S., Ríos, G., Rodríguez Almansa, A., Sánchez-Rodas, D., 2021 Removal of Sb Impurities in Copper Electrolyte and Evaluation of As and Fe Species in an Electrorefining Plant. Metals 11, 902.

Hait, J., Jana, R.K., Sanyal, S.K., 2009. Processing of copper electrorefining anode slime: a review. Mineral Proc. Extract, Metall. (trans. IMM c) 118, 240–252.

Hall, S., 1993. Gold and silver recovery from copper anode slimes at The Olympic Dam Joint Venture, Roxby Downs, SA. The Sir Maurice Mawby Memorial Volume. Australasian Mining and Metallurgy Monograph Series 19, 1102–1105.

Hoffmann, J.E., 2004. The Purification of Copper Refinery Electrolyte. JOM 56, 30–33.

Humphreys, F.J., 2001. Grain and subgrain characterisation by electron backscatter diffraction. J. Mater. Sci. 36, 3833–3854.

International Energy Agency (IEA), 2023 Final List of Critical Minerals 2022. https://www.iea.org/policies/15271-final-list-of-critical-minerals-2022 (accessed 30 May 2023).

Kanari, N., Allain, E., Shallari, S., Diot, F., Diliberto, S., Patisson, F., Yvon, J., 2019. Thermochemical route for extraction and recycling of critical, strategic and high value elements from by-products and end-of-life materials, Part I: Treatment of a copper by-product in air atmosphere. Materials 12, 1625.

Kanari, N., Allain, E., Shallari, S., Diot, F., Diliberto, S., Patisson, F., Yvon, J., 2020. Thermochemical route for extraction and recycling of critical, strategic and high-value elements from by-products and end-of-life materials, Part II: Processing in presence of halogenated atmosphere. Materials 13, 4203.

Khakmardan, S., Rezai, B., Abdollahzadeh, A., Ghorbani, Y., 2023. From waste to wealth: Unlocking the value of copper anode slimes through systematic characterization and pretreatment. Minerals Eng. 200, 108141.

Lane, D.J., Cook, N.J., Grano, S.R., Ehrig, K., 2016. Selective leaching of penalty elements from copper concentrates: A review. Minerals Eng. 98, 110–121.

Li, Z., Qiu, F., Tian, Q., Yue, X., Zhang, T., 2022. Production and recovery of tellurium from metallurgical intermediates and electronic waste - A comprehensive review. J. Cleaner Prod. 366, 132796.

Luo, D., Fernández de Labastida, M., Cortina, J.L., Lopez, J., 2023. Recovery of antimony and bismuth from arsenic-containing waste streams from the copper electrorefining circuit: An example of promoting critical metals circularity from secondary resources. J. Cleaner Prod. 415, 137902.

Mahmoudi, A., Shakibania, S., Mokmeli, M., Rashchi, F., 2020. Tellurium, from Copper Anode Slime to High Purity Product: A Review Paper. Metall. Mater. Trans. B 51, 2555–2575.

Mastyugin, S.A., Naboichenko, S.S., 2012. Processing of Copper-Electrolyte Slimes: Evolution of Technology. Russian J. Non-Ferrous Metals 53, 367–374.

McNulty, B.A., Jowitt, S.M., Belousov, I., 2022. The importance of geology in assessing by- and coproduct metal supply potential; a case study of antimony, bismuth, selenium, and tellurium within the copper production stream. Econ. Geol. 117, 1367–1385.

Mereiter, K., Preisinger, A., 1986 Kristallstrukturdaten der wismutminerale atelestit, mixit und pucherit Anzeiger der Osterreichische Akademie der Wissenschaften 123, 79-81.

Moats, M., Alagha, L., Awuah-Offei, K., 2021. Towards resilient and sustainable supply of critical elements from the copper supply chain: A review. J. Cleaner Prod. 307, 127207.

Moats, M.S., Filzwieser, A., Wang, S., Davenport, W.G., Robinson, T., Siegmund, A., 2019 Global Survey of Copper Electrorefining: 2019 World Tankhouse Operating Data. Proceedings, 58th Ann. Conf. of Metallurgists (COM) hosting the 10th Internat. Copper Conf., MetSoc.

Moats, M.S., Wang, S., Kim, D., 2012. A review of the behaviour and deportment of lead, bismuth, antimony and arsenic in copper electrorefining. In: Wang, S. (Ed.), T.T. Chen Honorary Symposium on Hydrometallurgy, Electrometallurgy and Materials Characterization. the Minerals. Metals and Materials Soc, Pittsburgh, PA, USA, pp. 3–21.

Mooney, R.C.L., 1948. Crystal structure of tetragonal bismuth arsenate, $BiAsO_4$. Acta Cryst 1, 163–165.

Nassar, N.T., Kim, H., Frenzel, M., Moats, M.S., Hayes, S.M., 2022. Global tellurium supply potential from electrolytic copper refining. Res., Conserv. Recycling 184, 106434.

Navarro, P., Alguacil, F.J., 2002. Adsorption of antimony and arsenic from a copper electrorefining solution onto activated carbon. Hydrometall. 66, 101–105.

Ojebuoboh, F., 2008. Selenium and Tellurium from Copper Refinery Slimes and their Changing Applications. World of Metallurgy - Erzmetall 61, 33–39.

Pennycook, S.J., Nellist, P.D., eds., 2011. Scanning Transmission Electron Microscopy. Imaging and Analysis. Springer, 762 pp.

Sawicki, J.A., Dutrizac, J.E., Friedl, J., Wagner, F.E., Chen, T.T., 1993. Mössbauer study of gold in a copper refinery. Nucl. Instr. Methods Phys. Res. B 76, 378–380.

Schlesinger, M.E., Sole, K.C., Davenport, W.G., Alvear Flores, G.R.F., 2021. Extractive Metallurgy of Copper, 6th edition,. Elsevier, p. 590 pp..

Schwartz, A.J., Kumar, M., Adams, B.L., Field, D.P., eds., 2000. Electron Backscatter Diffraction in Materials Science, 2nd edition. Springer, 406 pp.

Scott, J.D., 1990. Electrometallurgy of copper refinery anode slimes. Metall. Trans. B 21, 629–635.

Sejkora, J., Řídkošil, T., 1994 Tetrarooseveltite, β-Bi(AsO_4), a new mineral species from Moldava deposit, the Krušné hory Mts., Northwestern Bohemia, Czech Republic. N. Jahrb. Mineral. Monatsh. 179-184.

Steinlechner, S., 2018. Characterization and process development for the selective removal of Sn, Sb, and As from anode slime obtained from electrolytic copper refining. J. Mining Metall. B 54, 81–89.

Swinbourne, D.R., Barbante, G.G., Sheeran, A., 1998. Tellurium distribution in copper anode slimes smelting. Metall. Mater. Trans. B 29, 555–562.

Rio Tinto, 2022 Rio Tinto starts tellurium production at Kennecott https://www.riotinto.com/en/news/releases/2022/rio-tinto-starts-tellurium-production-at-kennecott (accessed 25 June 2023).

United States Geological Survey (USGS), 2014 Tellurium —The Bright Future of Solar Energy. Fact Sheet 2014 –3077, 2 pp.; http://minerals.usgs.gov.

Wang, X.W., Chen, Q.Y., Yin, Z.L., Xiao, L.S., 2006. Identification of arsenato antimonates in copper anode slimes. Hydrometall. 84, 211–217.

Wang, C., Li, S., Wang, H., Fu, J., 2016. Selenium minerals and the recovery of selenium from copper refinery anode slimes. J. s. African Inst. Mining Metall. 116, 593–600.

Xing, W.D., Sohn, S.H., Lee, M.S., 2019. A Review on the Recovery of Noble Metals from Anode Slimes. Mineral Proc. Extract. Metall. Rev. 41, 130–143.

Yang, P., Lee, S.S., Fenter, P., Bracco, J.N., Stack, A.G., 2023 Sorption of Arsenate, Selenate, and Molybdate on the Barite (001) Surface. ACS Earth Space Chem., in press; doi: 10.1021/acsearthspacechem.3c00096.

Zeng, Y., Liao, C., Liu, F., Zhou, X., 2023. Occurrence behaviors of As/Sb/Bi in copper anode slime and their separation by compound leaching followed by stepwise precipitation. ACS Omega 8, 10022–10029.

Zeng, H., Liu, F., Zhou, S., Liao, C., Chen, F., Zeng, Y., 2022. Leaching behavior of the main metals from copper anode slime during the pretreatment stage of the kaldor furnace smelting process. Processes 10, 2510.